Determination of Absolute Configuration of Natural Products: Theoretical Calculation of Electronic Circular Dichroism as a Tool

Xing-Cong Li*[,a,b], Daneel Ferreira [a,b] and Yuanqing Ding[a]

[a]*National Center for Natural Products Research, Research Institute of Pharmaceutical Sciences and* [b]*Department of Pharmacognosy, School of Pharmacy, The University of Mississippi, University, Mississippi 38677, USA*

Abstract: Determination of absolute configuration (AC) is one of the most challenging features in the structure elucidation of chiral natural products, especially those with complex structures. With revolutionary advancements in the area of quantum chemical calculations of chiroptical spectroscopy over the past decade, the time dependent density functional theory (TDDFT) calculation of electronic circular dichroism (ECD) spectra has emerged as a very promising tool. The principle is simply based on the comparison of the calculated and experimental ECD spectra: the more closely they match, the more reliable conclusion for the AC assignment can be drawn. This review attempts to use several examples representing monomeric flavonoids, rotationally restricted biflavonoids, complex hexahydroxydiphenoyl-containing flavonoids, conformationally flexible and restrained sesquiterpenoids, cembrane-africanene terpenoids, dihydropyranocoumarins, alkaloids, and dihydroxanthones to illustrate the applicability of this approach in determining the AC of structurally diverse natural products. The findings clearly indicate that the TDDFT calculation of ECD spectra can quantify the contribution of individual conformers and the interaction of multiple chromophores, making it possible to determine the AC of complex chiral molecules. The calculated electronic transitions and molecular orbitals provide new insight into the interpretation of ECD spectra at the molecular level.

Keywords: Absolute configuration, electronic circular dichroism, natural products, theoretical calculation, TDDFT.

1. INTRODUCTION

Natural products are an important source for drug discovery. Determination of absolute configuration (AC) is one of the most challenging tasks in the structure elucidation of chiral natural products, especially those with complex structures. The available methods include X-ray crystallography for crystalline compounds, chemical synthesis, NMR spectroscopy/chiral derivatization, analytical chemistry, and chiroptical approaches. Among these, X-ray crystallography probably remains the most powerful and effective approach, e.g., in the AC assignment of the antifungal agent amphotericin B [1]. In particular, the recent technology has made AC assignment possible without introduction of a heavy atom in the molecule [2-6]. However, this necessitates the availability of a suitable crystal, which is often difficult to obtain for some natural products, not to mention amorphous or liquid compounds. Chemical synthesis certainly provides convincing evidence, but is hampered by cost as shown in the total synthesis of the anticancer agent taxol [7,8] or is not applicable to all natural products. The NMR-based methods by preparing Mosher's esters [9,10] or using shift reagents [11,12] have been widely employed for the determination of the ACs of natural products due to convenience and easy access to the NMR instrument. Mosher's method requires the transformation of the chiral substrate by using a chiral derivatizing agent to afford diastereoisommers that can be differentiated by NMR spectroscopy. Analytical chemistry based methods via GC and HPLC analyses are particularly useful for the determination of the AC of the amino acid constituent units [13] of peptides and the sugar residues [14,15] of glycosides. Chiroptical methods involving empirical [16-20], semi-empirical [21], or non-empirical [22,23] rules have historically played an important role in determining the AC of natural products. Since each of the aforementioned methods has limitations, careful selection of an appropriate, or a combination of two or more methods, depending on the nature of the chiral molecule is crucial.

Electronic circular dichroism (ECD) has been demonstrated to be a powerful chiroptical tool for the AC assignment of natural products with various chromophores since the 1960s [24,25]. CD is the phenomena of a chiral molecule that adsorbs left and right circularly polarized light beams to a different extent. The difference of the absorptions is the measure of the magnitude of CD, which is expressed by the differential molar extinction coefficients as $\Delta\varepsilon = \varepsilon_l - \varepsilon_r$ ($L.mol^{-1}\cdot cm^{-1}$). The output of the CD instrument is usually expressed as molecular ellipticity θ, and the molar ellipicity $[\theta]$ can be correlated with $\Delta\varepsilon$ by the equation $[\theta] = 3300\,\Delta\varepsilon$. ECD is experimentally very sensitive and a non-destructive technique. A good spectrum can be obtained using 0.1-1 mg of the sample. The fundamentals of ECD have been reviewed previously [26-29]. Contrary to the phenomena of optical rotary dispersion (ORD) that any chiral molecule will show absorptions in the UV/vis wavelength range, appropriate chromophores such as carbonyl, diene, aromatic, or a conjugated system should be present in the molecule in order to exhibit measurable ECD absorptions or Cotton effects. In principle, chiral compounds with the same or similar chromophore(s) and stereochemical environment (including configuration and conformation) exhibit similar ECD spectra, which is the basis for the assignment of the AC of a new chiral molecule compared to those whose AC has been independently established by other methods such as X-ray crystallography or chemical synthesis. Several empirical sector rules drawn from the analysis of the ECD spectra of a large number of model compounds have been available and the octant rule [18,19] represents one of the most used for the prediction of AC of cyclohexanone derivatives. In addition, with theoretical evidence from quantum chemical calculations, the exciton chirality method [21] has been formulated as a semi-empirical rule to predict the AC of chiral molecules where two or more chromophores are *spatially coupled*. Nevertheless, ECD is primarily used

*Address correspondence to this author at National Center for Natural Products Research, Research Institute of Pharmaceutical Sciences, School of Pharmacy, The University of Mississippi, University, Mississippi 38677, USA; Tel: 662-915-6742; Fax: 662-915-7989. E-mail: xcli7@olemiss.edu

1385-2728/10 $55.00+.00 © 2010 Bentham Science Publishers Ltd.

as an empirical method for configurational assignment of natural products. It is very effective and reliable for the compounds with distinct chromophores and relatively simple stereogenic centers such as monomeric flavonoids [30]. For compounds with multiple chromophores and complex stereochemistry, the interpretation of ECD data in terms of AC is a complex exercise.

The past decade has witnessed revolutionary advancements in the area of quantum chemical calculations of ECD [31-39] as well as other chiroptical properties such as optical rotation [32,33,35-37,40-46] and vibrational circular dichroism (VCD) [47-54] using time dependent density functional theory (TDDFT), largely due to the improvement of the computational technologies. Compared to other methods such as coupled cluster theory and multiconfigurational self-consistent field theory [31,36,54,56] that are available for the theoretical calculation of ECD, TDDFT has been proved to provide a good fit in terms of the computational efforts and accuracy with regard to the experimental data, in particular for medium-sized molecules (molecular weight <1000) [38,57-61]. The calculated electronic transitions and molecular orbitals have allowed chemists to understand ECD at the molecular level. While on one hand the calculations can validate the previously deduced empirical rules, the most exciting aspect is that this approach seems to be able to determine the AC of any chiral molecule that produces a distinct experimental ECD spectrum. The principle is simply based on the comparison of the calculated and experimental ECD spectra: the more closely they match, the more reliable conclusion for the AC assignment can be drawn. Extensive studies on the application of the TDDFT method to the ECD calculation of chiral molecules, for example, of natural [5,34,35,38,39, 62-75] or synthetic [32,33,35-37,76-81] origin have been reported over the past few years. The purpose of this review is to use several examples representing different classes of natural products to illustrate the applicability of this approach in determining the AC of natural products.

2. COMPUTATIONAL METHODS

ECD calculations comprise two primary steps: conformational analysis to obtain the lowest energy conformers and subsequent calculations of the ECD spectra of the conformers. Initial systematic conformational search of a given molecule is generally carried out by using the MMFF94 molecular mechanics force-field method, e.g., via the SYBYL 8.1 program [82] and/or the AM1 and PM3 semiempirical methods, e.g., via the Spartan02 prgram [83]. Further geometric optimization of the resultant conformers is performed using the density functional theory (DFT) method, e.g., via the Gaussian03 program [84]. The best performing functionals for TDDFT calculations are the hybrid B3LYP, BH&HLYP, MPW1PW91, and PBE0, while the commonly used basis sets include polarization and possibly diffuse functions, for example, in order of size, 6-31G*, 6-31G**, 6-311G++**, aug-cc-pVDZ, and aug-cc-pVTZ [29, 57]. A large basis set may produce more reliable ECD results but requires longer computational time [85]. B3LYP/6-31G* generally performs well and is the choice for most TDDFT calculations. A molecule may afford more than one predominant conformer.

TDDFT at the same or a higher level is then employed to calculate excitation energy (in nm) and rotatory strength R (unit: 10^{-40} cgs) in the dipole velocity (R_{vel}) and dipole length (R_{len}) forms. "Self-Consistent Reaction Field" method (SCRF) with "COnductor-like continuum Solvent MOdel" (COSMO) [86-88] can be employed when taking the solvent effect [89,90] into consideration. The calculated rotatory strengths are simulated into an ECD curve by using the Gaussian function

$$\Delta\in(E) = \frac{1}{2.297\times10^{-39}}\frac{1}{\sqrt{2\pi\sigma}}\sum_{i}^{A}\Delta E_i R_i e^{-[(E-\Delta E_i)/(2\sigma)]^2}$$

where σ is the width of the band at 1/e height (typically in the range of 0.10~0.3 eV) and ΔE_i and R_i are the excitation energies and rotatory strength for transition i, respectively. Both the R_{vel} and R_{len} forms can be used for the simulation of the ECD spectrum, although the latter is considered to provide better results [31,85]. For multiple conformers, an overall ECD spectrum will be generated on the basis of Boltzman weighting of individual conformers. A more detailed theoretical basis for TDDFT calculations of ECD may be found in references 29, 31, and 57.

3. TDDFT CALCULATION OF ECD SPECTRA OF STRUCTUALLY DIVERSE NATURAL PRODUCTS

Structurally diverse chiral natural products containing different functionalities or chromophores that may produce a distinctive experimental ECD spectrum in the wavelength range of 200–400 nm are good targets for ECD calculation to determine AC. Conformationally rigid molecules, or molecules containing a single stereogenic center, or relatively simple chromophores, may quickly afford good calculated spectra. For conformationally flexible molecules, significant computational time is needed for comformational analysis. A prerequisite for ECD calculations is that the relative configuration or possible relative configuration of the stereogenic carbons near the chromophore of the molecule is known. It is understandable that CD can only sense the stereochemical difference near the chromophore in a molecule with multiple stereogenic centers. However, once the AC of one or two stereogenic carbons is determined by ECD calculation, the AC of the remaining stereogenic centers may be readily determined by NMR spectroscopy. More importantly, the attractiveness of the ECD calculation is that it can quantify the contribution of individual conformers and the interaction of multiple chromospheres, making it possible to determine the AC of complex chiral molecules. The following examples include natural products representing simple monomeric flavonoids, rotationally restricted biflavonoids, complex hexahydroxydiphenoyl-containing flavonoids, conformationally flexible and restrained sesquiterpenoids, cembrane-africanene terpenoids, dihydropyranocoumarins, alkaloids, and dihydroxanthones.

3.1. Flavonoids

CD may be the most powerful method in determining the AC of monomeric flavonoids [25]. Gaffield in 1970 demonstrated that (2*S*)-flavanone and (2*R*,3*R*)-3-hydroxyflavanone gave the same negative Cotton effect around 290 nm for their acetophenone π→π∗ transitions and a positive Cotton effect around 330 nm for their acetophenone n→π∗ transitions. Their enantiomers gave opposite Cotton effects. These CD patterns are the basis for all chiral flavonoids for AC assignment [30]. The simple monomeric flavanone (2*R*)-pinocembrin (**1**) and the flavanone glycoside mattucinol-7-*O*-*β*-D-glucopyranoside (**2**) were used as model compounds to provide theoretical evidence for the aforementioned interpretations and assess the feasibility and reliability of the TDDFT method in calculating ECD spectra of chiral flavonoids.

3.1.1. (2R)-Pinocembrin (1) [38]

(2*R*)-Pinocembrin (Fig. **1**) contains a single stereogenic center. The solid NMR evidence for this class of compounds indicates that

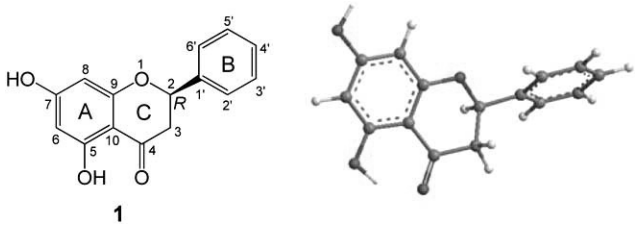

Fig. (1). Structure and optimized geometry of (2*R*)-pinocembrin (**1**) at the B3LYP/6-31G* level.

dominant conformer was located at the B3LYP/6-31G* level in the gas phase (Fig. **1**). The heterocyclic C-ring adopts a half-chair conformation with an equatorial phenyl B-ring rotated to be almost perpendicular to the the A/C-ring plane. The dihedral angle O1-C2-C1′-C2′ is 40.0°. The calculated total energies, important transitions, related rotatory strengths, and oscillator strengths of (2*R*)-**1** at the B3LYP/6-31G* level are shown in Table **1**, while the simulated ECD curve of (2*R*)-**1** is shown in Fig. (**2**). The calculated ECD spectrum is consistent with its experimental data in the region of 260-350 nm [91], although the maximum absorption is slightly shifted toward the low wavelength region, i.e., around 270 nm in the calculated ECD versus around 285 nm in the experimental ECD spectrum.

Table 1. Total Energies (au), Key Transitions and Their Related Rotatory and Oscillator Strengths of (2*R*)-pinocembrin (1) at the B3LYP/6-31G* Level

Species	Total Energy	Transition	ΔE^a (eV)	λ^b (nm)	f^c	$R_{vel}{}^d$	$R_{len}{}^e$
(2*R*)-**1**	–879.7254852	67→68	3.91	317	0.05	–10.3	–10.9
		65→68	4.12	301	0.01	13.8	14.8
		66→68	4.65	267	0.23	43.5	44.3
		63→68	4.99	249	0.01	–16.0	–16.8

[a] Excitation energy. [b] Wavelength. [c] Oscillator strength. [d] Rotatory strength in velocity form (10^{-40} cgs). [e] Rotatory strength in length form (10^{-40} cgs).

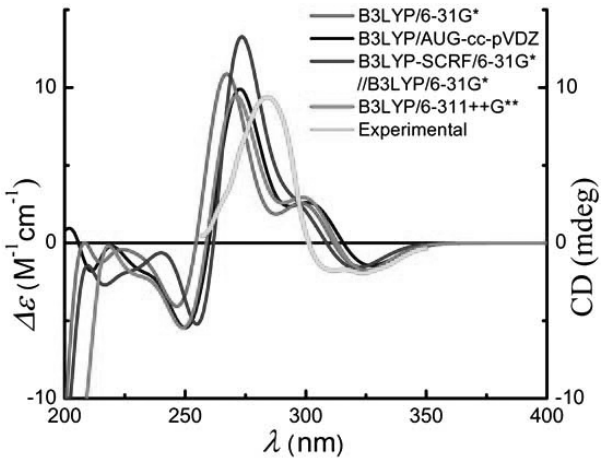

Fig. (2). Calculated ECD spectra of (2*R*)-pinocembrin (**1**) at different levels in $\Delta\varepsilon$ values (M^{-1} cm^{-1}) and its experimental ECD spectrum in the range of 260-350 nm in raw ellipiticiy (mdeg) [91].

the phenyl ring is equatorially oriented and the 5-OH forms an intramolecular hydrogen bond with the C4 carbonyl group. Thus, the conformational issue of this molecule is simple and only one pre-

For comparison purposes, the TDDFT calculations using different basis sets at the B3LYP/AUG-cc-pVDZ//B3LYP/6-31G* and B3LYP/6-311++G** levels, as well as at the B3LYP-SCRF/6-31G*//B3LYP/6-31G* level with the COSMO solution model were performed. The results showed that there are no major differences among the four simulated ECD curves. The positive rotatory strength at 267 nm calculated by B3LYP/6-31G* is slightly shifted toward the high wavelength region at 270 nm by B3LYP/6-311++G**, 272 nm by B3LYP/AUG-cc-pVDZ//B3LYP/6-31G*, and 272 nm by B3LYP-SCRF/6-31G*//B3LYP/6-31G*, which better fits with the experimental data at 285 nm in solution. However, when BHLYP/6-31G* and BLYP/6-31G* were employed, the calculated and experimental ECD spectra did not match. The above results indicate that TDDFT /B3LYP/6-31G* should be an effective method for calculating/predicting the ECD of monomeric flavonoids, with a larger basis set or consideration of the solvent effect further improving the method.

The molecular orbitals (MOs) involved in key transitions for the ECD of (2*R*)-**1** are shown in Fig. (**3**). The major positive rota-

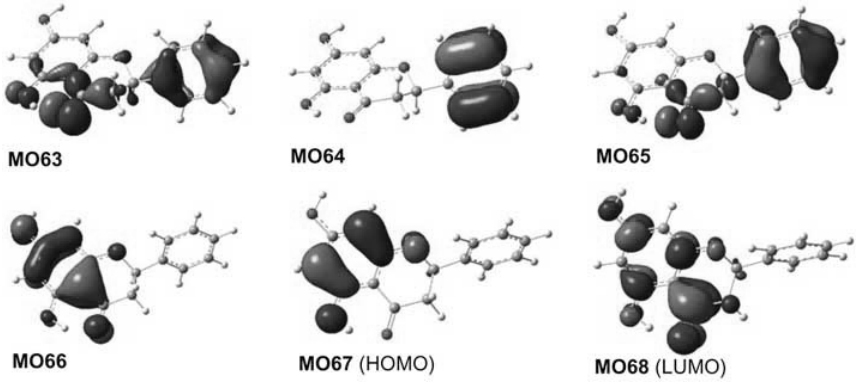

Fig. (3). Molecular orbitals involved in key transitions in the calculated ECD of (2*R*)-**1** at B3LYP/6-31G* level in gas phase.

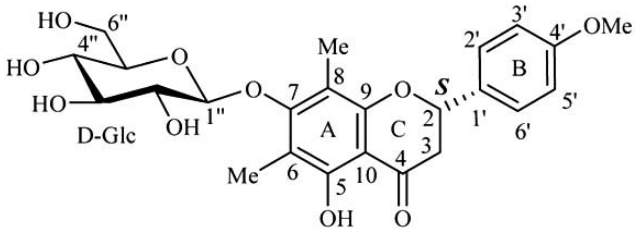

Fig. (4). Structure of mattucinol-7-*O*-*β*-D-glucopyranoside (**2**).

tory strength at 267 nm results from the electronic transition from MO66 involving a delocalized $^{14}_{11}\pi$ bonding (a fourteen-electron π system involving eleven atoms) of the acetophenone moiety to its corresponding unoccupied MO68 (LUMO). This supports the classical interpretation that the diagnostic positive Cotton effect in the range of 280-290 nm for this class of compounds is a contribution from the π → π* transition of the acetophenone moiety [30]. However, the observation that the negative rotatory strength at 317 nm resulted from the transition from HOMO (MO67), which excludes involvement of the electrons of the carbonyl group, to LUMO (MO68) contradicts the classical interpretation that the diagnostic Cotton effect around 330 nm for this class of compounds is associated with the acetophenone n → π* transition.

3.1.2. Mattucinol-7-O-β-D-glucopyranoside (2) [70]

Based on the conformational analysis of compound **1** supported by X-ray crystallographic data, a starting conformation with the B-ring almost perpendicular to the A/C-ring plane was set for compound **2** (Fig. **4**). The DFT method at the B3LYP/6-31G** level was performed to scan the potential energy surface of the conformers by rotating the glucosyl moiety about the C1"-O(C7) and (C1")O-C7 bonds to locate the stable points, affording 12 conformers. Further optimization at the B3LYP/6-31G** level relocated the eight stable conformers with key dihedral angles shown in Table **2**. Conformational analysis using relative free energies (ΔG) indicated the presence of four major conformers **2a1**, **2a2**, **2b1** and **2b2** with distributions of 33.4, 3.6, 60.0 and 2.9%, respectively, accounting for almost 100% in the gas phase, contributions of the remaining four conformers towards the conformational itinerary being insignificant. The glucosyl moiety is located above the A/C-ring plane in the **2a** series but below this plane in the **2b** series.

The calculated ECD spectra of conformers **2a1**, **2a2**, **2b1** and **2b2** in the gas phase by TDDFT at the B3LYP/6-31G** level are shown in Fig. (**5**). In addition, the calculations at the B3LYP/6-311++G**// B3LYP/6-31G**and B3PW91/6-31G**//B3LYP/6-31G** levels and the B3LYP-SCRF/6-31G**//B3LYP/6-31G** level in methanol solution with the COSMO model were performed. Overall, the calculated ECD spectra at the above levels were similar and consistent with the experimental spectrum. For example, the calculated negative rotatory strengths at 269 and 316 nm in **2a1** and those at 270 and 317 nm in **2b1** may contribute to the experimentally observed high-amplitude negative Cotton effect at 282 nm and a negative Cotton effect around 320 nm (shoulder), while the calculated positive rotatory strengths at 357 nm in **2a1** and 355 nm in **2b1** may be associated with the experimentally observed positive Cotton effect at 350 nm. The calculated MOs involved in the key transitions in **2b1** showed similar electron distributions as those of compound **1**. These results again suggest that TDDFT/B3LYP represents a feasible method for calculating/predicting the ECD of monomeric flavonoids.

3.2. Biflavonoids

3.2.1. Conformational Analysis of (+)-morelloflavone (3) [38]

The biologically active (+)-morelloflavone (**3**) (Fig. **6**) is a rotationally restricted flavanone-(3→8″)-flavone type of biflavonoid with two stereogenic centers and one chiral axis [92]. The NMR data and semiempirical AM1 calculations demonstrated that **3** possessed two preferred conformations about the interflavanyl bond in a ratio of 1:0.37 in solution, i.e. 73 to 27%. In the major and minor conformers **3a** and **3b**, respectively, the DEF-flavone moiety is extended above and below the plane of the A/C-ring of the ABC-flavanone moiety, respectively. It was assigned a 2*R*,3*S* absolute configuration based on comparison of its experimental CD with those of similar compounds [92]. ECD calculation of such a relatively large and comformationally flexible molecule to confirm the previous AC assignment represented a significant challenge.

Conformational search of the arbitrarily chosen (2*R*,3*S*)-**3** was conducted using the semiempirical AM1 method in the gas phase by rotating the DEF-flavone moiety with a step increase of the key dihedral angle, C4-C3-C8″-C7″, in which two stable conformers **3a** and **3b** with dihedral angles around 60 and 225° (i.e. –135°), re-

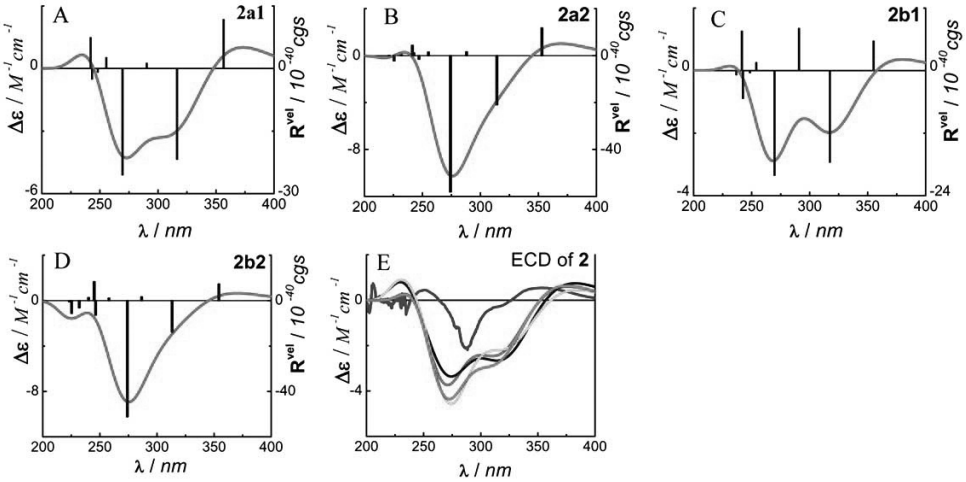

Fig. (5). Calculated ECD spectra of **2** in the gas phase at the B3LYP/6-31G** level (A→D), and its experimental and weighted ECD (E: ▬ experimental in MeOH; ▬ at the B3LYP/6-31G** level in the gas phase; ▬ at the B3LYP/6-311++G**//B3LYP/6-31G** level in the gas phase; ▬ at the B3PW91/6-31G**//B3LYP/6-31G** level in the gas phase; ▬ at the B3LYP-SCRF/6-31G**//B3LYP/6-31G** level with COSMO in MeOH).

Table 2. Important Dihedral Angles in Conformers of 2 (deg)

	2a1	2a1′	2a1″	2a2	2b1	2b1′	2b1″	2b2
C1"-O-C7-C6	102	96	107	56	–79	–89	–79	–126
C2"-C1"-O-C7	164	–80	–20	119	163	–80	–23	118
O1-C2- C1′- C2′	–43	–43	–43	–43	–40	–38	–40	–43

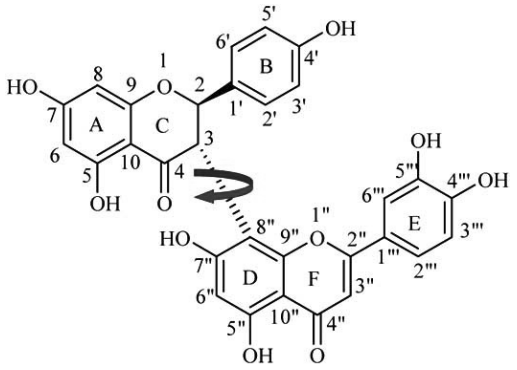

Fig. (6). Structure of the rotationally restricted morelloflavone (**3**).

spectively, were obtained based on its potential energy surface. For the major conformer **3a**-series, a further search using the AM1 method by rotating the unsymmetric E-ring of the DEF-flavone moiety and considering the presence or absence of a hydrogen bond between C7″-OH and the C4 carbonyl group afforded eight conformers **3a1**–**3a8**. Note that **3a1**–**3a4** have hydrogen bonding between C7″-OH and the C4 carbonyl group. In a similar way, the minor conformer **3b**-series also gave eight conformers **3b1**–**3b8**. Optimization of individual conformers were then performed at the B3LYP/6-31G* level and harmonic frequencies analysis at the same level conducted to confirm these minima. Stable points on the potential energy surfaces for **3a1**–**3a8** and **3b1**–**3b4** were relocated, but for **3b5**–**3b8**, only two minima, **3b5** and **3b7**, were obtained. Among these conformers, the key dihedral angles of C4-C3-C8″-C7″ vary from 50 to 61° in **3a1**–**3a8**, –80 to –83° in **3b1**–**3b4**, and –126 and –131° in **3b5** and **3b7**, respectively.

Since strong interactions between the multiple hydroxy groups in these conformers and the solvent may have a considerable influence on their minimum energies and possibly further affecting the ECD calculations, the single point energy (SPE) of every conformer in methanol was calculated at the B3LYP-SCRF/6-31G*//B3LYP/6-31G* level with the COSMO model. An interesting finding was that the total energy of conformer **3b7** both in the gas phase and in methanol was considerably lower than those of all others due to the formation of the hydrogen bond of C3‴-OH···O-C5 and inclusion of this conformer in the conformational analysis will result in a population of almost 100%, excluding the presence of all other conformers. **3b7** is the only conformer that possesses the hydrogen bonding between C3‴-OH and C5-OH. However, it is reasonably perceived that this loose intramolecular hydrogen bond is unlikely to survive due to the rotating nature of the bulky flavanyl moieties and strong interaction between the C7″-OH and the solvent. Hence, the C7″-OH that is presumably solvated has little chance to form a hydrogen bond with the C5-OH since the two flavanyl moieties are dynamically rotating to preclude a *frozen* conformer at that critical point. Thus, this unusual conformer **3b7** *ideally* generated by the theoretical models should not be significant in solution in real time. Surprisingly, the exclusion of **3b7** has made the conformational analysis using the SPEs of the remaining conformers in methanol in close agreement with the experimental data: a total of 73.9% population for major conformers **3a1**–**3a8** and 26.1% population for minor conformer **3b1**–**3b5** versus experimentally observed 73 to 27% for major and minor conformers (Table **2**). Only four major conformers **3a5** (23.4%), **3a6** (30.8%), **3a7** (3.5%), and **3a8** (15.2%) and one minor conformer **3b5** (26.1%) are predominant (Fig. **7**). The conformational analysis using ΔE, $\Delta E'$, or ΔG in the gas phase did not match the experimental data (Table **2**). It appears that consideration of the solvent effect is critical for the conformational analysis of such molecules and appropriate judgment should be exercised when dealing with certain *negative* theoretical data in a complex situation.

3.2.2. ECD of (+)-morelloflavone (3)

Based on the conformational analysis of **(+)-3** in solution, the ECD spectra of conformers **3a5**–**3a8** and **3b5** were calculated using TDDFT and the COSMO model at the B3LYP-SCRF/6-31G*//B3LYP/6-31G* level and are shown in Fig. (**8**). While there

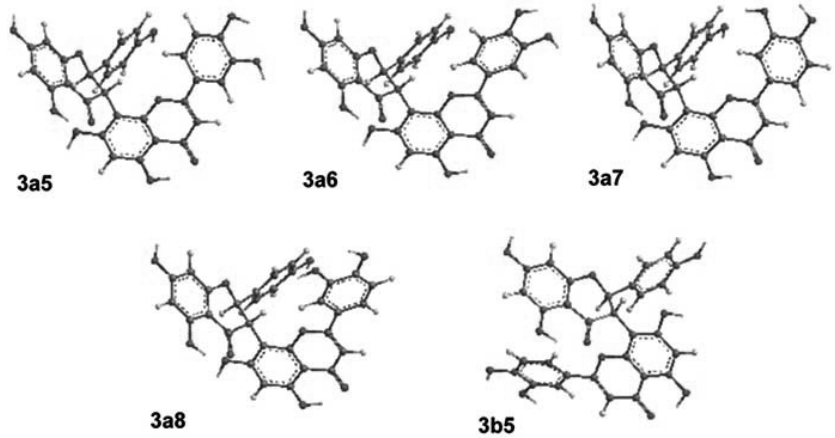

Fig. (7). Optimized geometries of conformers of (2*R*,3*S*)-**3** at the B3LYP/6-31G* level in the gas phase.

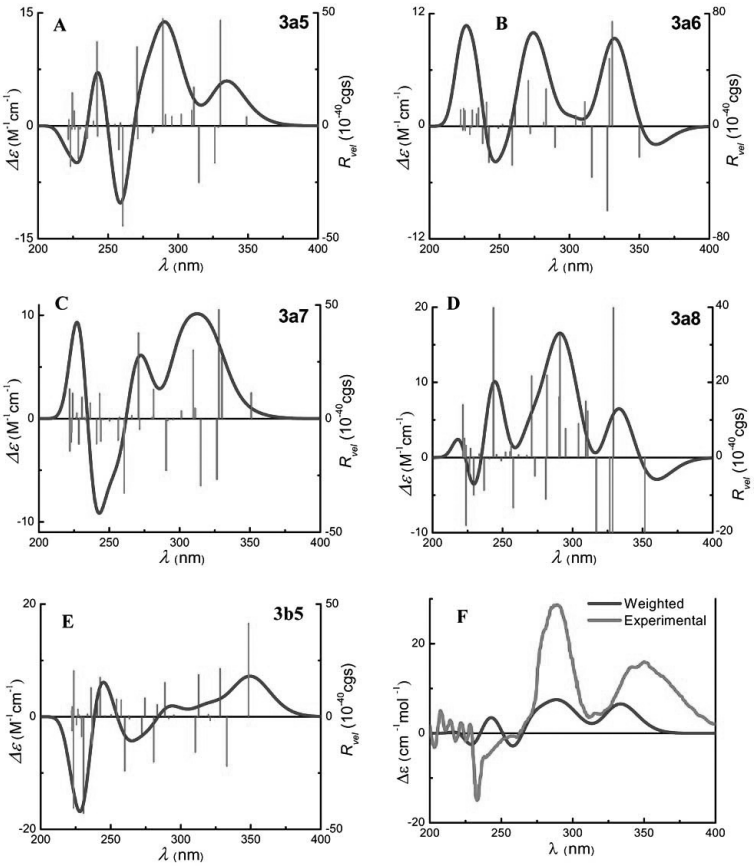

Fig. (8). Calculated ECD spectra of conformers **3a5**–**3a8** and **3b5** (A→E) by TDDFT at the B3LYP-SCRF/6-31G*//B3LYP/6-31G* level in methanol and their weighted ECD (F) and the experimental ECD spectrum of (+)-**3** in methanol (F).

Table 3. Conformational Analysis of (2*R*,3*S*)-3 in the Gas Phase and in Methanol Solution

Species	In Gas Phase						In Methanol	
	ΔE^a	$P_E\%^b$	$\Delta E'^c$	$P_{E'}\%^d$	ΔG^e	$P_G\%^f$	ΔEs^g	$P_{Es}\%^h$
3a1	0.41	10.0	0.39	7.8	1.30	3.2	2.86	0.3
3a2	0.00	19.8	0.02	14.7	1.07	4.7	2.44	0.5
3a3	0.67	6.4	0.51	6.4	0.88	6.5	3.85	0.1
3a4	0.11	16.6	0.00	15.2	0.63	9.9	2.87	0.2
3a5	0.53	8.2	0.23	10.2	0.78	7. 7	0.16	23.4
3a6	0.64	6.7	0.32	8. 9	0.39	14.7	0.00	30.8
3a7	0.43	9.6	0.15	11.8	0.00	28.6	1.29	3.5
3a8	0.37	10.5	0.08	13.3	0.25	18.7	0.42	15.2
3b1	2.84	0.2	3.06	0.1	4.15	0.0	4.84	0.0
3b2	5.12	0.0	5.17	0.0	5.77	0.0	8.42	0.0
3b3	2.52	0.3	2.71	0.2	3.34	0.1	6.42	0.0
3b4	4.85	0.0	5.04	0.0	6.11	0.0	6.99	0.0
3b5	0.31	11.7	0.16	11.5	0.93	5.9	0.10	26.1

[a,c,e] Relative energy, relative energy with *ZPE*, and relative Gibbs free energy, respectively (kcal/mol). [b,d,f] Conformational distribution calculated by using the respective parameters above at the B3LYP/6-31G* level in the gas phase. [g,h] Relative energy (kcal/mol) and conformational distribution at the B3LYP-SCRF/6-31G*//B3LYP/6-31G* level with COSMO model in methanol solution, respectively.

are differences between these conformers, conformer **3a5** (23.4%) shows positive Cotton effects around 285 and 340 nm (Fig. **8A**), which is very similar to the experimental ECD spectrum in methanol displaying positive Cotton effects around 290 and 350 nm (Fig. **8F**). The two conformers, **3a6** (30.8%), and **3a8** (15.2%), also produce positive Cotton effects around 285 and 340 nm (Fig. **8B** and **8D**). Conformer **3b5** (26.1%) representing the minor conformer series produces a strong Cotton effect around 350 nm (Fig. **8E**),

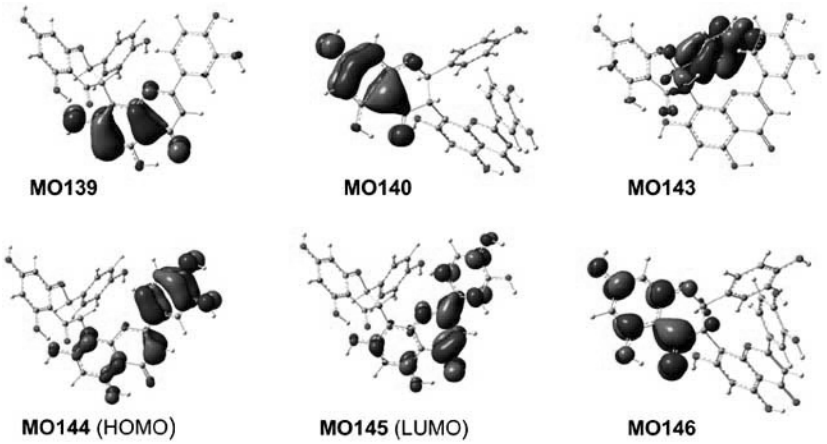

Fig. (9). Molecular orbitals involved in key transitions in the calculated ECD spectrum of **3a5** at the B3LYP-SCRF/6-31G*//B3LYP/6-31G* level in methanol.

Table 4. Key Transitions and Their Related Oscillator and Rotatory Strengths in the ECD Spectra of (2*R*,3*S*)-Morelloflavone Conformers 3a5 and 3b5 at the B3LYP-SCRF/6-31G*//B3LYP/6-31G* Level

Transition	ΔE^a (eV)	λ^b (nm)	f^c	$R_{vel}{}^d$	$R_{len}{}^e$
3a5					
143→145	3.75	330	0.089	46.9	50.5
139→145	4.29	289	0.094	47.5	48.3
140→146	4.58	271	0.347	35.0	31.5
3b5					
144→145	3.56	348	0.309	41.5	47.6
143→145	3.78	328	0.137	21.5	24.2
143→146	3.96	313	0.043	18.8	17.7
139→145	4.29	289	0.077	15.2	15.1

[a] Excitation energy. [b] Wavelength. [c] Oscillator strength. [d] Rotatory strength in velocity form (10^{-40} cgs). [e] Rotatory strength in length form (10^{-40} cgs).

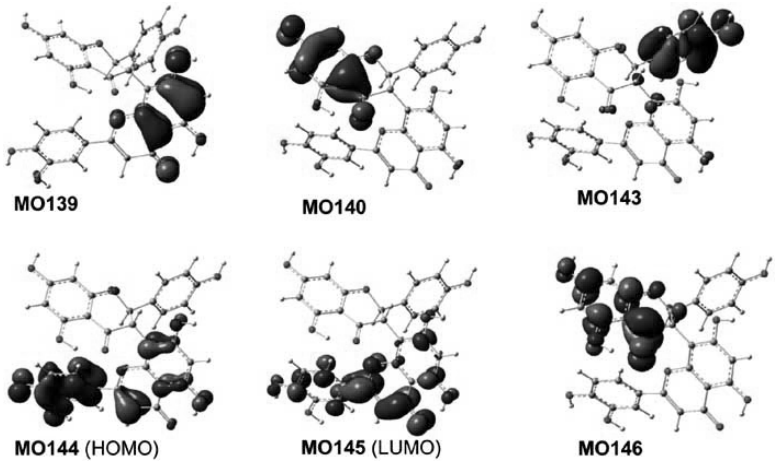

Fig. (10). Molecular orbitals involved in key transitions in the calculated ECD of conformer **3b5** at the B3LYP-SCRF/6-31G*//B3LYP/6-31G* level in methanol.

which may complement the positive Cotton effect around 340 nm produced by the major conformers **3a5**, **3a6**, and **3a8**. A weighted ECD curve based on the populations of the above five conformers is finally generated as shown in Fig. (**8F**), which is overall consistent with the experimental ECD in methanol, particularly for the two diagnostic Cotton effects around 290 and 350 nm. Therefore, it can be convincingly concluded that the (2*R*,3*S*)-absolute configuration assigned to (+)-**2** on the basis of empirical rules is correct.

Analysis of the calculated ECD spectrum of the representative conformers **3a5** and **3b5** has provided an understanding of the generation of the experimentally observed ECD spectrum of this compound at the molecular level. Table **4** lists the key transitions, oscillator strengths, and rotatory strengths of conformers **3a5** and **3b5**, while the molecular orbitals involved in the key transitions are shown in Figs. (**9** and **10**). Table **4** showed that the experimentally observed Cotton effect around 290 nm in **3** is contributed by the

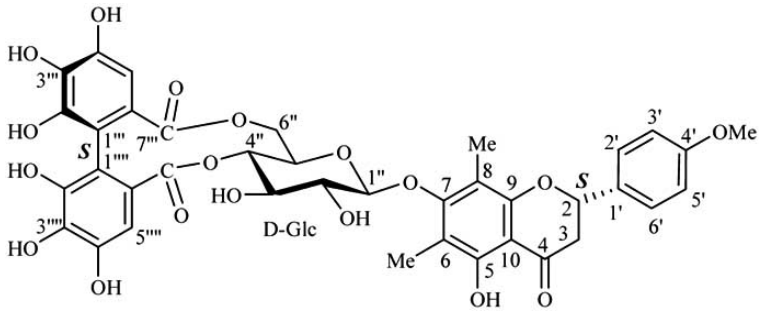

Fig. (11). Structure of mattucinol-7-*O*-[4",6"-*O*-(*aS*)-hexahydroxydiphenoyl]-*β*-D-glucopyranoside (**4**).

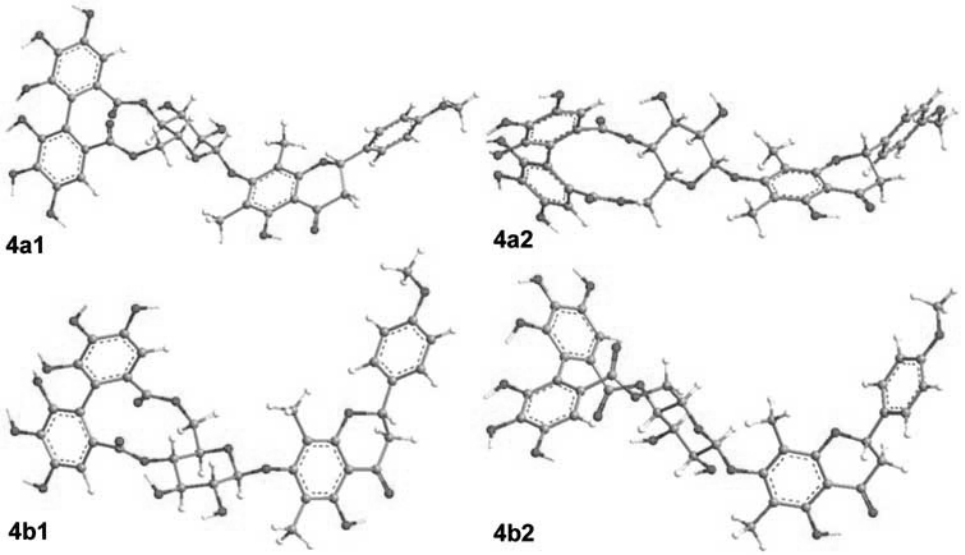

Fig. (12). Major conformers of optimized geometries of compound **4** at the B3LYP/6-31G** level in the gas phase.

positive rotatory strengths at 271 and 289 nm in **3a5**, resulting from the transitions from MO140 to MO146 and from MO139 to MO145, respectively. The former corresponds to the acetophenone $\pi \rightarrow \pi^*$ transition of the ABC-flavanone moiety, similar to the monomeric flavonoid pinocembrin (**1**) discussed above, while the latter generating an even stronger positive rotatory strength is associated with the electronic transition within the DEF-flavone moiety. The diagnostic positive Cotton effect around 350 nm in the experimental ECD would be contributed by the positive rotatory strength at 330 nm generated from the transition from MO143 to MO145 that reflects the electronic interaction between the ABC-flavanone moiety via the B-ring π electrons and the DEF-flavone moiety in major conformer **3a5**, which is further strengthened by the positive rotatory strength at 348 nm from the transition of MO144 to MO145 that involves the electrons within the DEF-flavone moiety in **3b5**. The results indicate that the electronic interaction between the ABC-flavanone and DEF-flavone moieties plays a critical role in generating the aforementioned two positive Cotton effects. This supports an empirical interpretation that the positive Cotton effect around 350 nm for morelloflavone may be produced by the electronic transitions of the achiral DEF-flavone moiety chirally perturbed by the ABC-flavanone moiety [93].

The calculated ECD spectra of conformers **3a1**–**3a8**, **3b5**, and **3b7** using TDDFT at the B3LYP/6-31G* level in the gas phase are conspicuously not in agreement with the experimental ECD. This strongly suggests that the utilization of the B3LYP-SCRF method with the solution COSMO model is critical. The solvent effect apparently plays a pivotal role in the case of **3** containing multiple hydroxy groups capable of forming inter- and intra-unit hydrogen bonds when compared with the monomeric pinocembrin (**1**) that bears fewer hydroxy groups and produces a calculated ECD spectrum in solution similar to that in the gas phase (Fig. **2**). It is also interesting to note that the calculated ECD spectra of **3b7** with the COSMO model at the B3LYP-SCRF/6-31G*//B3LYP/6-31G* and B3LYP-SCRF/6-31G* levels do not match the experimental ECD spectrum of **3**, supporting the conjecture that **3b7** does not play a significant contributing role in solution.

3.3. Hexahydroxydiphenoyl-Containing Flavonoids

Mattucinol-7-*O*-[4",6"-*O*-(*aS*)-hexahydroxydiphenoyl]-*β*-D-glucopyranoside (**4**) [70] (Fig. **11**) is a *Candida* secreted aspartic protease inhibitor isolated from the plant *Miconia myriantha* [94]. The hexahydroxydiphenoyl (HHDP) moiety is an essential stereogenic element of ellagitannins, a group of natural products widely distributed in plants. Composed of flavanone, *β*-D-glucopyranosyl, and (*aS*)-HHDP structural moieties, this relatively bulky molecule is considered to be an ideal model to examine the roles of the three structural moieties in generating its overall ECD spectrum by TDDFT calculations.

The experimental ECD spectrum of **4** showed a high-amplitude positive Cotton effect around 240 nm, a low-amplitude negative Cotton effect in the 260-300 nm region, and a minor positive Cotton effect around 350 nm (Fig. **13E**). With consideration of the additive ECD contribution of the HHDP and flavanone structural moieties in conjunction with the empirical rules [30,95], the former

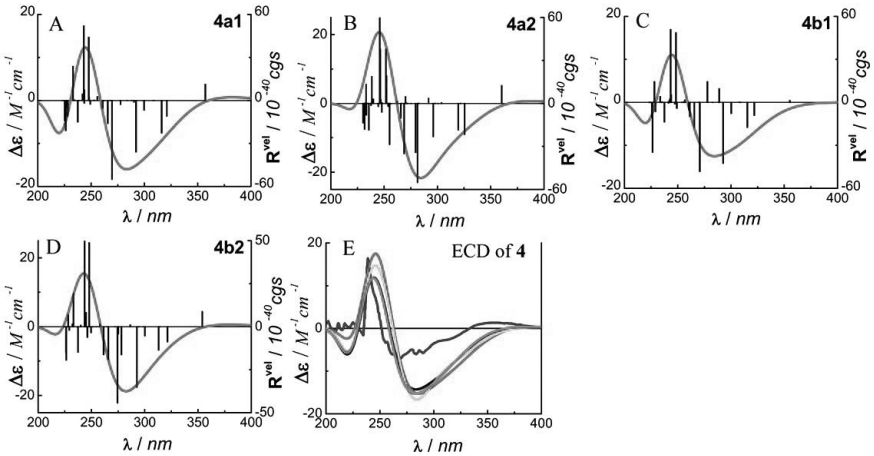

Fig. (13). Calculated ECD spectra of **4** in the gas phase at the B3LYP/6-31G** level (A→D), and its experimental and weighted ECD in MeOH (E: ▬ experimental in MeOH; ▬ at the B3LYP/6-31G** level in the gas phase; ▬ at the B3LYP/6-311++G**//B3LYP/6-31G** level in the gas phase; ▬ at the B3PW91/6-31G**//B3LYP/6-31G** level in the gas phase; ▬ at the B3LYP-SCRF/6-31G**//B3LYP/6-31G** level with COSMO in MeOH).

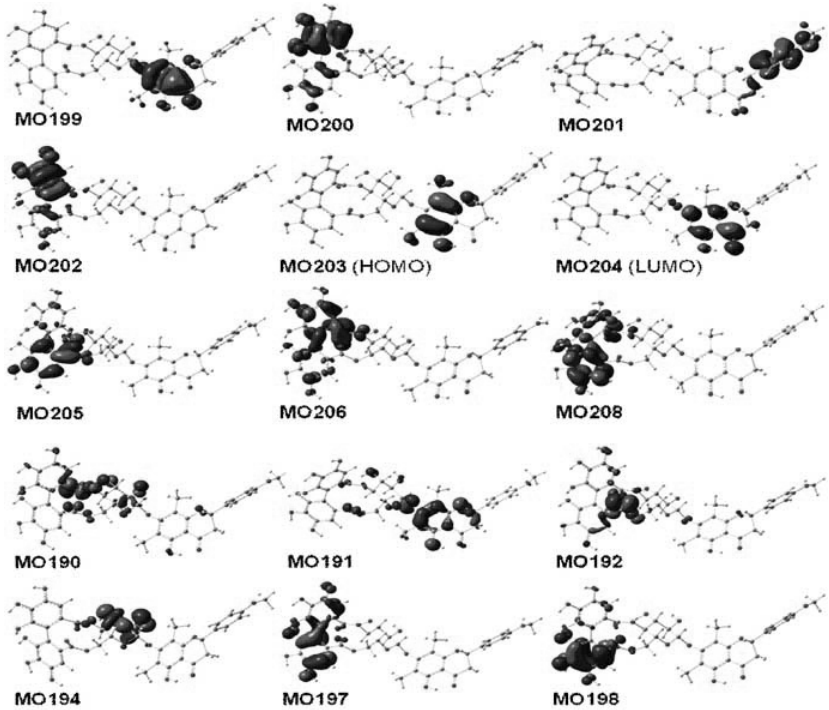

Fig. (14). Molecular orbitals involved in key transitions generating ECD spectrum of **4a1** at the B3LYP/6-31G** level in the gas phase.

was assigned *aS* and the latter 2*S* configuration. The theoretical calculation of the ECD of **4** was based on this assumption.

The optimized geometries of compound **2** were the basis for the conformational search of compound **4**. Once the (*aS*)-HHDP group is attached to the *β*-D-glucopyranosyl moiety, the conformational flexibility of the two structural moieties is limited thus simplifying the geometric optimization. Similarly, only four conformers **4a1** (52.1%), **4a2** (2.8%), **4b1** (43.0%) and **4b2** (2.0%) (Fig. **12**) were obtained with significant distributions at the B3LYP/6-31G** level by Gibbs free energy in the gas phase in which the flavanone and glucosyl moieties adopt conformations similar to **2a1**, **2a2**, **2b1** and **2b2**, respectively. The dihedral angle C2‴-C1‴-C1⁗-C2⁗ of the (*aS*)-HHDP moiety in these conformers is 57°.

The ECD calculations of conformers **4a1**, **4a2**, **4b1** and **4b2** were carried out by the TDDFT method at the B3LYP/6-31G** level in the gas phase. The transitions, related rotatory strengths, and oscillator strengths of one major conformer, **4a1**, are shown in Table **5**. The simulated ECD of the four conformers and their weighted ECD spectra are shown in Fig. (**13**). The calculated and experimental ECD spectra are in good agreement. The experimentally observed positive Cotton effect at 240 nm in **4** may result from the two high-amplitude positive rotatory strengths around 245 nm in the four conformers, while the low-amplitude negative Cotton effect from 260-300 nm is contributed by a series of negative rotatory strengths, e.g., at 266, 270, 292, 316, and 321 nm in **4a1**. The low-amplitude positive Cotton effect around 350 nm may be contributed mainly by the positive rotatory strength at 357 nm in **4a1** since the positive rotatory strength at 355 nm in another major conformer **4b1** is negligible and the contributions from the two minor conformers **4a2** and **4b2** would be very small.

Table 5. Key Transitions and Oscillator and Rotatory Strengths of Conformer 4a1 at the B3LYP/6-31G Level in the Gas Phase**

Transition	ΔE^a (eV)	λ^b (nm)	f^c	R_{vel}^d	R_{len}^e
203→204	3.47	357	0.063	11.2	13.3
202→205	3.86	321	0.044	–11.0	–19.2
201→204	3.92	316	0.013	–22.6	–24.3
202→206	4.24	292	0.075	–35.9	–39.9
199→204	4.60	270	0.277	–55.0	–56.8
197→205	4.67	266	0.019	–16.0	–17.9
198→206	4.98	249	0.035	–2.5	–12.7
202→208	5.00	248	0.088	44.0	44.8
197→206	5.10	243	0.038	51.8	56.6
192→205	5.22	237	0.014	–15.0	–17.7
200→208	5.32	233	0.149	23.7	39.0
190→206	5.480	226.3	0.017	–20.9	–21.9
194→205	5.483	226.1	0.012	–15.3	–15.3
191→204	5.50	225	0.012	–14.0	–13.6

[a] Excitation energy. [b] Wavelength. [c] Oscillator strength. [d] Rotatory strength in velocity form (10^{-40} cgs). [e] Rotatory strength in length form (10^{-40} cgs).

The calculated MOs of conformer **4a1** (Fig. **14**) involved in the contributions to the aforementioned rotatory strengths, reveals the roles of the (*aS*)-HHDP and (2*S*)-flavanone moieties in generating the overall ECD of this molecule. The (*aS*)-HHDP moiety not only generates the two strong positive rotatory strengths at 243 nm (MO197 to MO206) and 248 nm (MO202 to MO208) but also three strong negative rotatory strengths at 266 nm (MO197 to MO206), 292 nm (MO202 to MO206), and 321 nm (MO202 to MO205). The latter three negative rotatory strengths synergize the two negative rotatory strengths from the (2*S*)-flavanone moiety at 270 nm (MO199 to MO204) and 316 nm (MO201 to MO204) contributing a broad Cotton effect in the 260-300 nm region. The positive rotatory strength at 357 nm (MO203 to MO204) of the (2*S*)-flavanone moiety represents the contribution of the diagnostic Cotton effect at the longer wavelength. In this case, it appears that the two chromophores have simple additive effects to the overall ECD spectrum and the original configurational assignment of **4** based on the empirical rules is thus confirmed.

To examine the reliability of the ECD calculation of **4** at the B3LYP/6-31G** level, single point energies of each conformer were calculated at the B3LYP/6-311++G**//B3LYP/6-31G** level in the gas phase, at the B3LYP-SCRF/6-31G**//B3LYP/6-31G** level with the COSMO model in MeOH, and at the B3PW91/6-31G**//B3LYP/6-31G** level in the gas phase. Minor changes for conformational distribution of conformers **4a1**:**4a2**:**4b1**:**4b2** were observed among the three levels, changing to 47.6:2.3:48.5:1.5%, 37.3:8.9:45.1:8.5%, and 45.2:8.2:45.1:8.5%, respectively. However, the calculated ECD spectra of each conformer at the above three levels were largely similar to the ones obtained by B3LYP/6-31G** in the gas phase. The weighted ECD spectra are shown in Fig. (**13**). Again, this indicates that the TDDFT with the modest basis set B3LYP/6-31G** would be a sufficient method for theoretical ECD calculation of flavonoids, in particular for dealing with relatively bulky naturally occurring compounds.

It is expected that the glucopyranosyl moiety has little effect on the ECD spectrum of mattucinol-7-*O*-*β*-D-glucopyranoside (**2**), as evidenced by the calculated ECD spectrum of mattucinol-7-*O*-*β*-L-glucopyranoside showing similar spectrum to that of **2** [70]. However, it would be interesting to probe the role of the glucopyranosyl moiety (as a linker between the two chromophores) in generating the ECD spectrum of **4**. Thus, the *β*-D-glucopyranosyl unit in **4** was replaced with a *β*-L-glucopyranosyl moiety in the hypothetical mattucinol-7-*O*-[4",6"-*O*-(*aS*)-hexahydroxydiphenoyl]-*β*-L-glucopyranoside. The calculated ECD spectrum of this compound is similar to that of **4**, indicating that the AC of the glucopyranosyl unit has little effect on their ECD [70]. Thus, the AC of the sugar residues in similar glycosides will have to be determined by other methods.

To further examine the interacting effect of the HHDP and the flavanone moieties, ECD calculation of a hypothetical compound mattucinol-7-*O*-[4",6"-*O*-(*aR*)-hexahydroxydiphenoyl]-*β*-D-glucopyranoside was performed at the B3LYP/6-31G** level [70]. As expected, the major rotatory strengths around 240 nm from the (*aR*)-HHDP moiety were reversed with a negative sign. However, the major rotatory strength at 270 nm of the (2*S*)-flavanone moiety in **4a1** was also reversed with a positive sign. The electronic interaction between the (2*S*)-flavanone and (*aR*)-HHDP moieties also produces two positive rotatory strengths, resulting in an overall broad positive Cotton effect in the 260-300 nm region. Assuming the experimental and calculated ECD spectra are similar, an erroneous 2*R* configuration may be assigned for the flavanone moiety based on the empirical rule requiring a positive Cotton effect in the 260-300 nm region. The complex interaction between chromophores in chiral molecules of this class clearly precludes ECD interpretation by simple empirical rules.

3.4. Sesquiterpenoids

3.4.1. Cycloabiesesquine A (5) [72]

Cycloabiesesquine A (**5**), isolated from the plant *Abies delavayi*, represents a conformationally flexible sesquiterpenoid. Conformational analysis and ECD calculations using the TDDFT method played a critical role in the structure elucidation of this novel natural product.

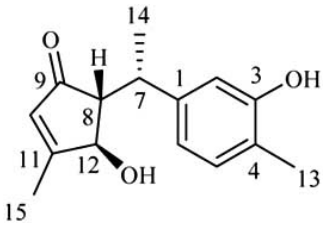

Fig. (15). Structure of cycloabiesesquine A (**5**).

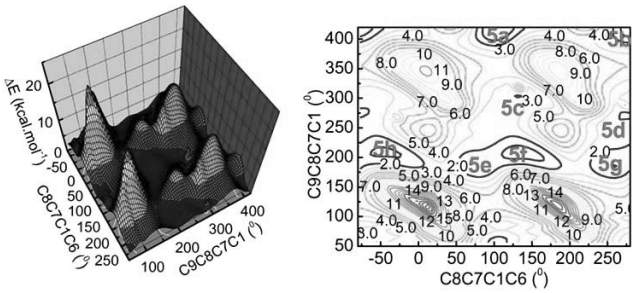

Fig. (16). Potential energy surface of **5** at the AM1 level in the gas phase (left: 3D color map surface; right: contours).

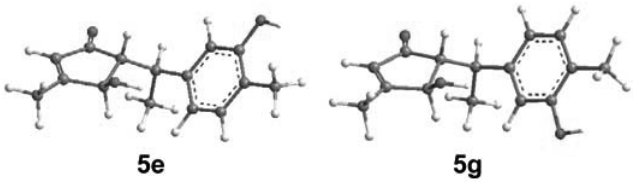

Fig. (17). Optimized geometries of predominant conformers **5e** and **5g** of compound **5** at the B3LYP/6-31G** level in the gas phase.

The relative configuration of compound **5** was initially deduced on the basis of NMR spectroscopy (Fig. **15**). The potential energy surface of **5** was scanned at the AM1 level by rotating about the C8-C7 and C7-C1 bonds, resulting in eight minimum energy points (Fig. **16**). All eight conformers (**5a–5h**) were relocated and confirmed at the B3LYP/6-31G** level. The single point energy in the gas phase at the B3LYP/6-311++G**//B3LYP/6-31G** level and in methanol solution at the B3LYP-SCRF/6-31G**//B3LYP/6-31G** level with the COSMO model were also calculated. Conformational analysis indicated that conformers **5e** and **5g** are predominantly populated: **5e** accounts for 32–47% of conformations in the gas phase and 36% in methanol solution, while **5g** represents 50–61% in the gas phase and 30% in methanol solution. The only difference between **5e** and **5g** is the orientation of the aromatic ring due to free rotation (Fig. **17**). Both conformers are consistent with the observed NOE correlations and the small coupling constants between H-8 and H-12 (2.4 Hz) and between H-7 and H-8 (4.2 Hz) are in accord with calculated dihedral angles.

ECD spectra of conformers **5a–5h** were calculated at the B3LYP/6-31G** and B3LYP/6-311++G**//B3LYP/6-31G** levels in the gas phase, and at the B3LYP-SCRF/6-31G**//B3LYP/6-31G** level with the COSMO model in methanol solution. It is important to note that only the predominant conformers **5e** and **5g** generated ECD spectra similar to the experimental ECD spectrum of **5**. The weighted spectra of the eight conformers at the three levels are shown in Fig. (**18**). Overall, the calculated ECD spectra showed diagnostic negative and positive Cotton effects around 330 and 235 nm, respectively, consistent with the experimental ECD spectrum. Thus, the structure of **5** was unequivocally determined as (7*S*,8*R*,12*R*)-4,8-dihydroxy-1,3,5,10-tetraen-8,12-cyclobisabolan-9-one.

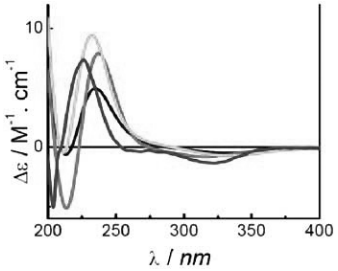

Fig. (18). Calculated and experimental ECD spectra of compound **5** (— at the B3LYP/6-31G** level in the gas phase; — at the B3LYP-SCRF/6-31G**// B3LYP/6-31G** level with the COSMO model in MeOH; — at the B3LYP/6-311++G**//B3LYP/6-31G** level in the gas phase; — experimental in MeOH).

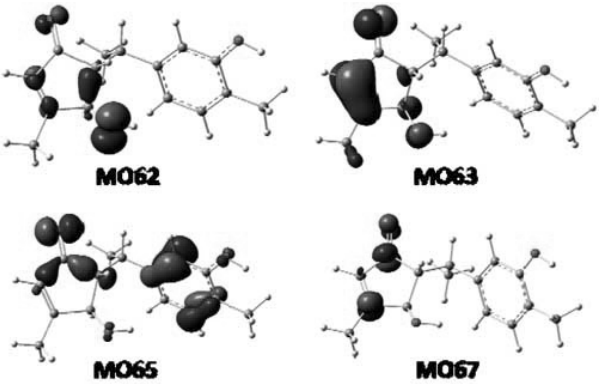

Fig. (19). Molecular orbitals involved in the key transitions in the ECD spectrum of conformer **5e** at the B3LYP-SCRF/6-31G**//B3LYP/6-31G** level with the COSMO model in MeOH.

MO analysis of conformers **5e** and **5g**, at the B3LYP-SCRF/6-31G**//B3LYP/6-31G** level with the COSMO model in MeOH, provided comprehension of the production of the experimentally observed ECD spectrum of **5** at the molecular level. The electronic transitions from MO62 and MO63 to MO67 involving the electrons of the α,β-unsaturated ketone moiety in the cyclopentenone system (Fig. **19**) afford positive rotatory strengths at 234 nm in both **5e** and **5g**, which are consistent with the strong positive Cotton effect at 226 nm in the experimental ECD spectrum of **5**. The electronic transition from MO65 to MO67 contributes to the negative rotatory strengths at 321 nm in both **5e** and **5g**, which are associated with another diagnostic negative Cotton effect at 322 nm in the experimental ECD spectrum of **5**.

3.4.2. Quadrone A (6) [62]

The cytotoxic compound quadrone A (**6**), isolated from the fungus *Aspergillus terreus*, represents a conformationally rigid sesquiterpenoid (Fig. **20**). The X-ray crystallographic data of this compound was available and its AC was determined by total synthesis as 1*R*, 2*R*,5*S*,8*R*,11*R*. This is a good model compound to demon-

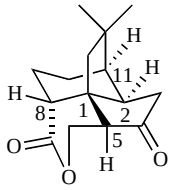

Fig. (20). Structure of quadrone (**6**).

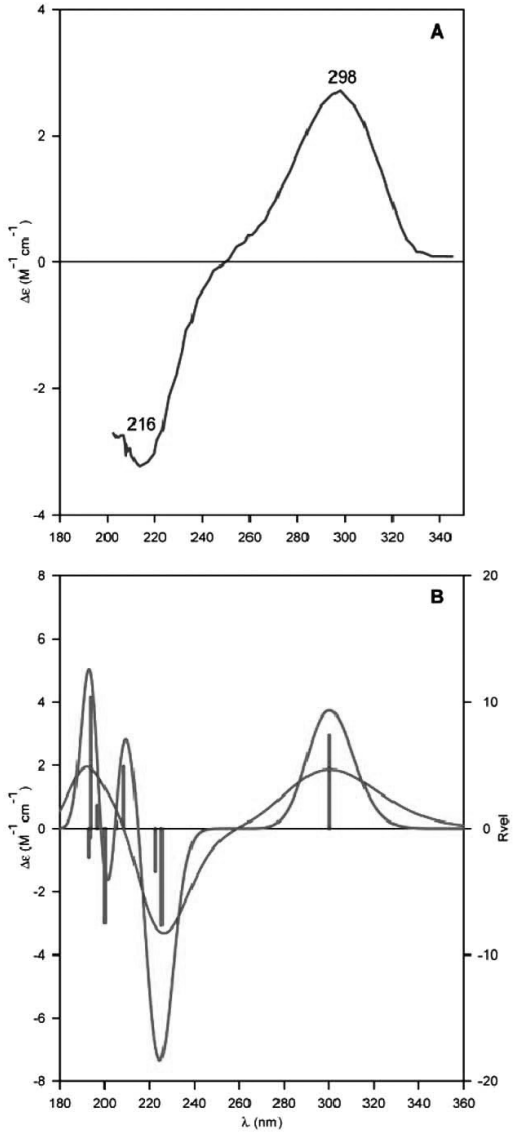

Fig. (21). Experimental ECD spectrum of compound **6** in MeOH (A) and its calculated velocity representation B3LYP/augcc-pVDZ//B3LYP/6-31G* rotational strengths and simulated ECD spectrum (red line, σ = 0.2 eV; green line, σ = 0.4 eV). Reprinted with permission from ref. [62]. Copyright 2006 American Chemical Society.

strate the reliability of the TDDFT calculation of its ECD spectrum for AC assignment.

Initial conformational analysis of **6** was carried out using Monte Carlo searching together with the MMFF94 molecular mechanic force field. All stable conformations obtained were then optimized using DFT at the B3LYP/6-31G* level, affording three stable conformations. Using the B3LYP/6-31G* relative free energy, the most stable conformation was predicted to be >99%, i.e., there is only one single conformation for the molecule. The cyclohexane ring has a chair conformation, while the lactone ring has a boat conformation. The cyclopentanone ring is nonplanar. The calculated dihedral angles at the B3LYP/6-31G* level are very similar to those obtained from the X-ray crystallography.

Next, TDDFT calculations of the ECD spectrum of **6** at the B3LYP/aug-cc-pVDZ level based on the B3LYP/6-31G* geometry were performed. Plots of the rotatory strengths against the wavelength and the simulated ECD spectrum are shown in Fig. (**21**). The calculated and experimental spectra are in good agreement over the relatively limited spectral range of the experimental spectrum. The positive Cotton effect at 298 nm and the negative Cotton effect at 216 nm are reproduced by the calculations. The lowest energy excitation, i.e., the n $\rightarrow\pi^*$ transition of the ketone group, contributes to the diagnostic Cotton effect at 298 nm. This calculation is consistent with the previous AC assignment for **6** by chemical synthesis. In this work [62], the authors further calculated the ORD and VCD spectra of this compound, providing convincing evidence to demonstrate the power of theoretical calculation of chiroptical spectroscopy in determining the AC of this compound.

3.5. Cembrane-Africanene Terpenoids

Cembrane-africanene terpenoids [5] are a small of group of natural products comprising a conformationally flexible macrocyclic cembrane diterpenoid structural moiety and an africanene sesquiterpene unit. The structure elucidation of 7*E*-polymaxenolide (**7**) and 7*E*-5-epipolymaxenolide (**8**) (Fig. **22**) isolated from the hybrid soft coral *Sinularia maxima* × *S. polydactyla* presents an interesting case of the successful utilization of the TDDFT calculation of their ECD spectra [5].

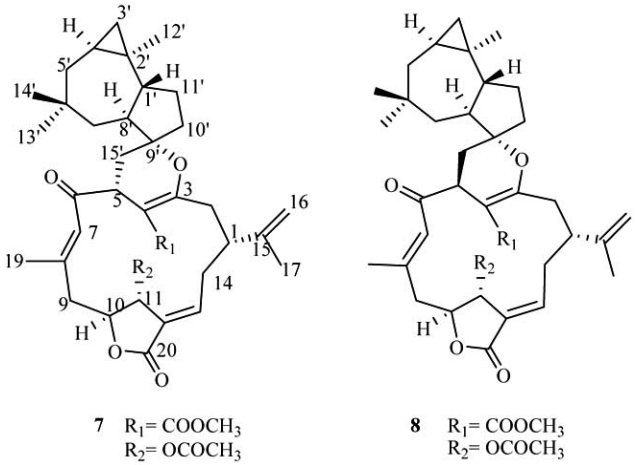

Fig. (22). Structures of 7*E*-polymaxenolide (**7**) and 7*E*-5-epipolymaxenolide (**8**).

Initial X-ray crystallographic analysis determined the relative configuration of compound **7**. On the basis of the X-ray coordinates, a starting conformation for **7** was constructed and optimized at the B3LYP/6-31G** level. It should be noted that an extensive conformational search for such a conformationally flexible molecule would require excessive computational time. Subsequent ECD calculation at the B3LYP-SCRF/6-31G**//B3LYP/6-31G** level afforded an ECD spectrum similar to the experimental one (Fig. **23**), permitting determination of the AC of the compound. This was further confirmed by refinement of the structure using low-temperature (90K) X-ray diffraction data from a Bruker Kappa Apex-II diffractometer equipped with CuKα radiation, and was based on resonant scattering of the light atoms only, principally oxygen. It should be pointed out that despite the similarities between the calculated and experimental ECD spectra, differences are evidenced by the larger amplitude of the short wavelength Cotton effect near 220 nm in the calculated ECD spectrum presumably resulting from minor conformational differences between the calculated and solution conformers.

In the case of compound **8** which is configurationally different from **7** only at C5, the starting conformation was based on the optimized conformation of **8** at the B3LYP/6-31G** level. Geometric optimization at this level and subsequent ECD calculation at the B3LYP-SCRF/6-31G**//B3LYP/6-31G** level produced a simulated ECD spectrum very close to the experimental one (Fig. **23**), confirming the AC assignment for this compound.

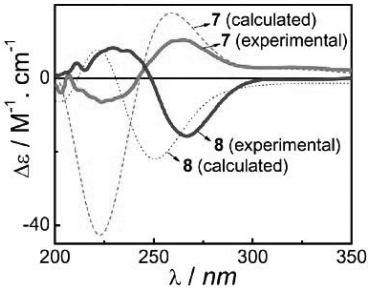

Fig. (23). Calculated and experimental ECD spectra of compounds **7** and **8** at the B3LYP-SCRF/6-31G**//B3LYP/6-31G** level.

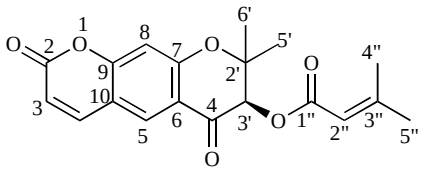

Fig. (24). Structure of scuteflorin A (**9**).

Reversing the C5 configuration led to almost opposite experimental ECD spectra for **7** and **8**. Superficially, the calculated and experimental spectra of **7** and **8** may be interpreted such that these compounds are indeed enantiomers. However, comparison of the minimum energy conformers of **7** and **8** indicates the dramatic conformational changes, and hence vastly different chiroptical properties resulting from inversion of configuration at C5. Dreiding models and the energy-minimized molecular model of **8** clearly indicate that inversion of configuration at C5 realigns the electronic transition dipole moments of the exocyclic α,β-unsaturated lactone and ketone chromophores to now reflect negative exciton chirality [21] and hence 5*S* as opposed to 5*R* configuration in compound **7**.

3.6. Dihydropyranocoumarins

Scuteflorin A (**9**) (Fig. **24**) is a new dihydropyranocoumarin isolated from the plant *Scutellaria lateriflora*. The AC of the single stereogenic center at C-3' was determined using TDDFT calculations, with the contributions to the overall ECD spectrum of this compound from the dihydro-γ-pyranone-containing coumarin chromophore and the senecioyl chromophore being defined [73].

The potential energy surface of **9** in the gas phase was scanned at the AM1 level by rotating about the C3′-O, C1″-O (C3′), and C1″-C2″ bonds. Six conformers were found and redefined at the B3LYP/6-31G** level. Conformational analysis indicated that conformer **9a** is predominant [95.6% at the B3LYP/6-31G** level in the gas phase by Gibbs free energies and 95.9% at the B3LYP-SCRF/6-31G**//B3LYP/6-31G** level in methanol by total energies]. TDDFT calculation of the ECD of **9a** was performed at the B3LYP/6-31G** and B3LYP/AUG-ccpVDZ//B3LYP/6-31G** levels in the gas phase and at the B3LYPSCRF/6-31G**//B3LYP/6-31G** level in methanol. The calculated ECD spectra of **9a** in the gas phase and in methanol, together with the

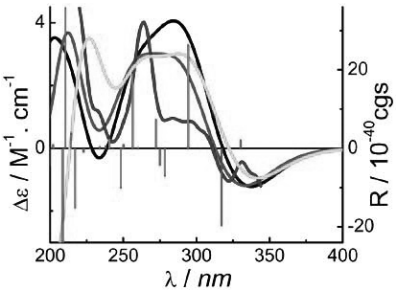

Fig. (25). Calculated ECD spectra of conformer **9a** and the experimental ECD of compound **1** (red ▬ and olive ▬, in the gas phase at the B3LYP/6-31G** level; black ▬, in MeOH solvent at the B3LYP-SCRF/6-31G**//B3LYP/6-31G** level with COSMO; green ▬, in the gas phase at the B3LYP/AUG-cc-pVDZ//B3LYP/6-31G** level; blue ▬, experimental ECD in MeOH).

experimental ECD curve of **1** in MeOH, are shown in Fig. (**25**). The overall patterns of the calculated ECD spectra were consistent with that of the experimental one, i.e., a positive and negative Cotton effects in the 250-300 and 300-350 nm regions, respectively. Considering the extended π-system of the dihydro-γ-pyranone containing coumarin chromophore in **9**, the positive Cotton effect near 260 nm and the shoulder near 290 nm in the experimental ECD spectrum would be characteristic for this molecule. This was supported by analysis of the MOs involved in key transitions generating the ECD spectrum of **9a** at the B3LYP/6-31G** level in the gas phase. The calculated positive rotatory strength at 272 nm, which likely contributes to the positive Cotton effect near 260 nm in the experimental ECD spectrum, originates via the transitions from MO88 to MO91 (Fig. **26**). Another calculated positive rotatory strength at 294 nm, indicative of the shoulder near 290 nm in the experimental ECD spectrum, is derived from the transition from MO90 to MO92. The calculated negative rotatory strength at 317 nm, which may be associated with the negative Cotton effect beyond 300 nm in the experimental ECD spectrum, is generated by the transition from MO90 to MO91. All four MOs involve the π-electrons in the dihydro-γ-pyranone containing coumarin chromophore. The calculated positive rotatory value at 257 nm, which originates via the transition from MO86 to MO93, also contributed to the positive Cotton effect near 260 nm in the experimental ECD spectrum. The strong calculated positive rotatory value at 210 nm results from the transition from MO87 to MO93. Since these three MOs involve the electrons of the α,β-unsatuated ester system that may rotate along the C3′-O (C1″), C1″-O (C3′), and C1″-C2″ bonds in solution, caution should be exercised in using the Cotton effects near these wavelengths to predict AC.

3.7. Alkaloids

3.7.1. Discorhabdins [68]

Enantiomeric pairs of the cytotoxic pyrroloiminoquinone marine alkaloids discorhabdins B (**11**), G*/I (**12**), L (**13**), and W (**14**) (Fig. **27**) were isolated from *Latrunculia* species sponge collected at different locations around the coast of New Zealand. TDDFT calculations of their ECD spectra are particularly suitable for the determination of the AC of this class of compounds, including conformationally ridgid **11**–**13** and the conformationally flexible **14** [68].

The feasibility and reliability of the TDDFT method on this class of compounds was first demonstrated by the calculation of the ECD spectrum of (+)-(5*R*,6*S*,8*S*)-discorhabdin/prianosin A (**10**), the AC of which was previously defined by X-ray crystallography

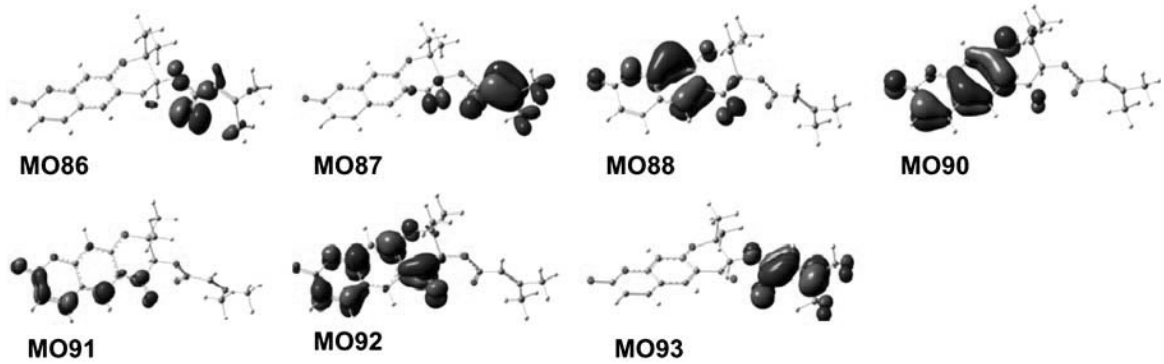

Fig. (26). Molecular orbitals involved in key transitions in the ECD spectrum of **9a** at the B3LYP/6-31G** level in the gas phase.

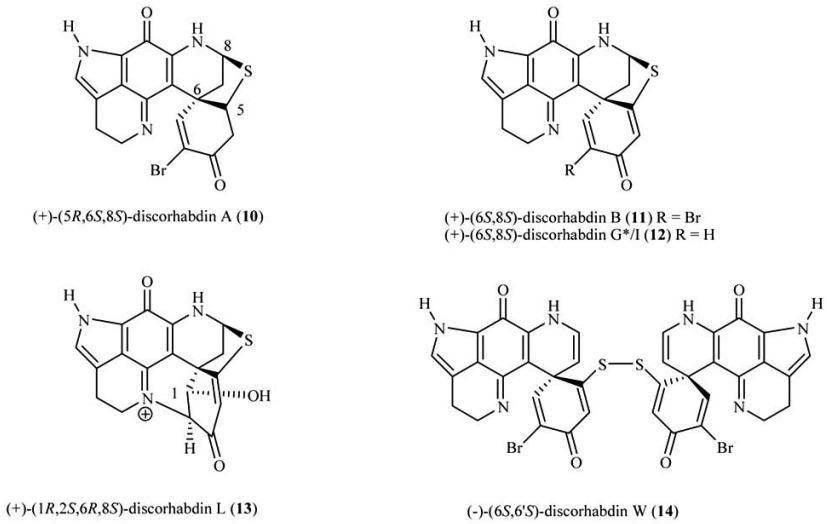

Fig. (27). Structures of discorhabdins.

analysis. The geometry of **10** was based on its crystal structure and optimized at the B3LYP/6-31G** level, affording a single optimized conformer. The ECD calculations of **10** were then conducted in the gas phase at the B3LYP/6-31G** level and further in methanol at the B3LYP-SCRF/6-31G**//B3LYP/6-31G** level. The calculated and experimentally observed ECD spectra are in excellent agreement (Fig. **28**).

Due to structural similarities between these compounds, the starting conformations of **11**–**13** were constructed on the basis of the optimized geometry of **10**. In fact, there is only one predominant conformer optimized at the B3LYP/6-31G** level for each compound. Minor differences for the experimental ECD spectra were observed for the free base and trifluoroacetate salt of **11**, and calculations were thus performed on both forms. The calculated ECD spectrum of the salt is a better match than the free base (Fig. **29**). For compounds **12** and **13**, only the ECD spectra of their salts were calculated, which are also in good agreement with the experimental ones (Fig. **30**).

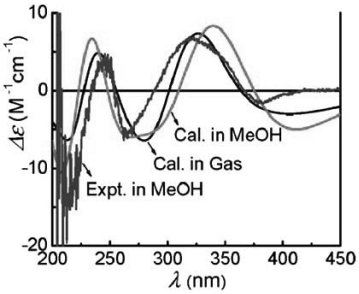

Fig. (28). Calculated ECD spectra (σ = 0.20 eV) of (+)-(5*R*,6*S*,8*S*)-discorhabdin A (**10**) at the B3LYP/6-31G** level in the gas phase and the B3LYP-SCRF/6-31G** level in methanol compared to the experimental spectrum.

(–)-(6*S*,6'*S*)-Discorhabdin W (**14**) is presumably derived from (+)-discorhabdin B (**11**) via light-promoted dimerization. A conformational search was done at the AM1 level by rotating the C5-S(S-C5') and (C5-S)S-C5' bonds. Conformational analysis at this level afforded a predominant conformation with a population of 96%, which was used for the ECD calculation. The calculated and experimental spectra are overall consistent (Fig. **31**), confirming the AC assignment of this dimeric discorhabdin.

A more recent study on the TDDFT calculation of the ECD spectrum of a new discorhabdin analogue, discorhabdin Y from the deep-water Alaskan sponge *Latrunculia* sp., also resulted in an unequivocal assignment of its AC [96].

3.7.2. Actinophyllic Acid (15) [74]

(–)-Actinophyllic acid (**15**) is a novel alkaloid isolated from the tree *Alstonia actinophylla* as a carboxypeptidase U inhibitor. It has an unprecedented 2,3,6,7,9,13c-hexahydro-1*H*-1,7,8-(methanetriyloxymethano)pyrrolo[1′,2′:1,2]azacino[4,3-*b*]indole-8(5*H*)-carbox-

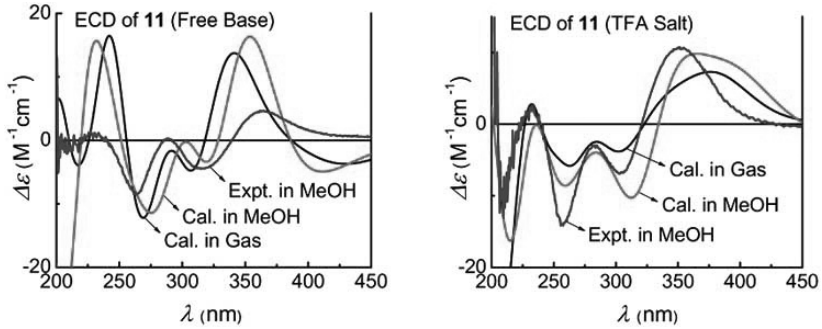

Fig. (29). Calculated ECD spectra (─ B3LYP/6-31G** level; ─ at the B3LYP-SCRF/6-31G** level) for (6*S*,8*S*)-discorhabdin B (**11**) in gas phase, methanol solvation model compared to experimental spectrum observed for (+)-**11** (blue) as either free base or trifluoroacetate salt.

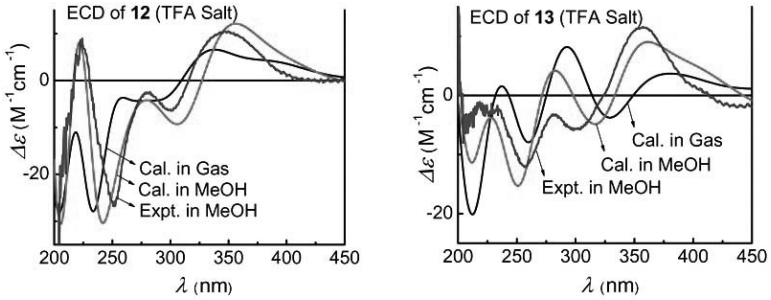

Fig. (30). Calculated and experimental ECD spectra of (6*S*,8*S*)-discorhabdin G*/I (**12**) and (1*R*,2*S*,6*R*,8*S*)-discorhabdin L (**13**) as their trifluoroacetate salt (─ B3LYP/6-31G**; ─ at B3LYP-SCRF/6-31G**).

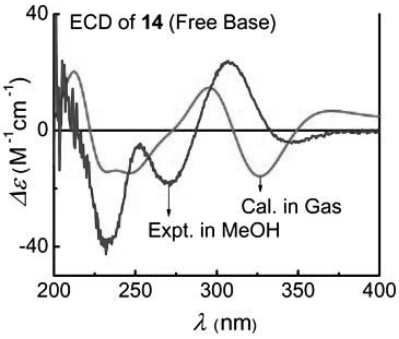

Fig. (31). Calculated (B3LYP/6-31G** level in gas phase) and experimental ECD spectra of (6*S*,6'*S*)-discorhabdin W (**14**).

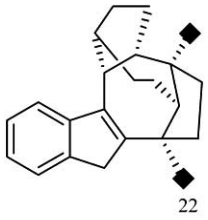

15 R = H
15a R = Me

Fig. (32). Structures of (–)-actinophyllic acid (**15**) and its methyl ester (**15a**).

ylic acid skeleton. Its relative configuration was confirmed by the total synthesis of (±)-**15**. To reduce the intermolecular interaction with solute and solvent molecules that may change spectroscopic properties, its carboxylic ester, (–)-**15a** (Fig. **32**) was prepared and used for ECD calculations [74].

The initial structure for the calculation was arbitrarily presented as (15*R*,16*S*,19*S*,20*S*,21*R*)-**15a**, the enantiomer deduced by the proposed biosynthetic pathway starting with tryptamine and (−)-secologanin glucoside. An MMFF94 Monte Carlo search yielded only two conformers that differ in the orientation of the C22 ester group within a 10 kcal/mol window. Optimization of these conformers at the DFT/B3LYP/6-31G(d,p) level without considering solvent effects did not change these geometries significantly. Conformers **15a1** and **15a2** (Fig. **33**) constitute 91.4 and 8.6%, respectively, of the conformational itinerary.

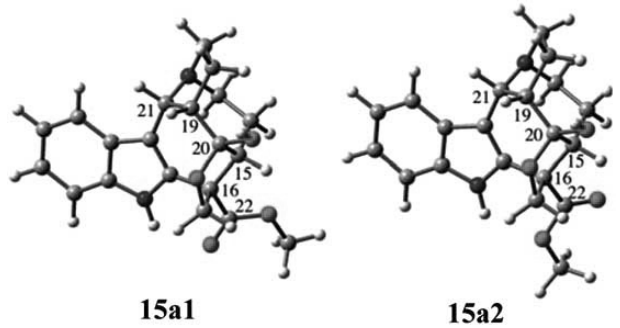

Fig. (33). Two stable conformers of (15*R*,16*S*,19*S*,20*S*,21*R*)-**15a** optimized at the B3LYP/6-31G(d,p) level. Reprinted with permission from ref. [74]. Copyright 2009 American Chemical Society.

TDDFT calculations of the ECD spectrum of the two conformers were performed at the B3LYP/6-31G(d,p) and B3LYP/augcc-pVDZ levels. The theoretical spectrum by 6-31G(d,p) matched the experimental spectrum for (–)-**15a**: a negative broad band around 275 nm, an upward tendency close to zero around 240 nm, and a negative Cotton effect around 210 nm (Fig. **34**). The spectrum calculated at aug-cc-pVDZ reproduced the negative shoulder around 230 nm well, although the upward region around 240 nm became weakly positive. The calculations confirmed the 15*R*,16*S*,19*S*,20*S*, 21*R*-configuration of (-)-**2**, consistent with the conclusions deduced from theoretical calculation of its optical rotation [74].

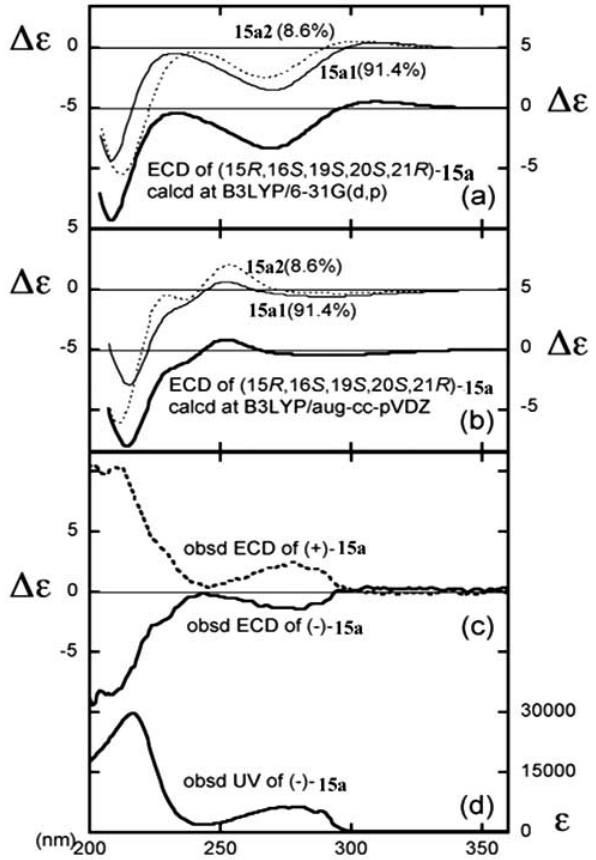

Fig. (34). (a) Calculated ECD spectra of (15*R*,16*S*,19*S*,20*S*,21*R*)-**15a** at the B3LYP/6-31G(d,p) and (b) at the B3LYP/aug-cc-pVDZ levels. (c) Observed ECD and (d) UV spectra of **15a** in methanol (0.25 mM). Reprinted with permission from ref. [74]. Copyright 2009 American Chemical Society.

3.7.3. Shichizozygine (16) [64]

(+)-Schizozygine is one of a group of alkaloids that have been isolated from the East African plant *Schizozygia caffaeoides.* It can have either the 2*R*,7*S*,20*S*,21*S* AC as shown in Fig. (**35**) or 2*S*,7*R*,20*R*,21*R*, and was thus subjected to ECD calculation for configurational assignment.

A Monte Carlo conformational search using the MMFF94 molecular mechanics force field identified two conformations, **16a** and **16b** (Fig. **36**), **16a** being lower in energy than **16b**. Conformations **16a** and **16b** differ principally with regard to the conformation of ring C, which adopts boat and chair conformations, respectively. The geometries of conformations **16a** and **16b** were then optimized at the B3LYP/6-31G* level, indicating that ring-F of **16a** and **16b** is oppositely puckered, in contrast to the starting conformation obtained at the MMFF94 level where ring-F is close to planar. Thus, a potential energy surface scan at the B3LYP/6-31G* level, varying the dihedral angle C9-C10-O-C24 for both conformations **16a** and **16b** was performed, affording additional conformations, **16a'** and **16b'**, respectively. Further conformational search at the B3LYP/6-31G* level, varying the dihedral angles C2-C21-C20-C19, C21-C2-C7-C6, C2-C21-N-C5, and C20-C21-N-C3, for conformations **16a** and **16b** did not yield additional conformers. The geometries of the four conformations were reoptimized at the B3LYP/TZ2P and B3PW91/TZ2P levels, and vibrational frequencies calculated. At all levels, the percentage populations of conformations **16a** and **16a'** are 35-40% and the populations of conformations **16b** and **16b'** are 10-15%. It is important to note that such a seemingly conformationally rigid molecule afforded four conformations via a careful conformational search.

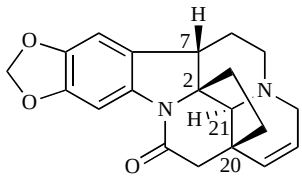

Fig. (35). Structure of shichizozygine (**16**).

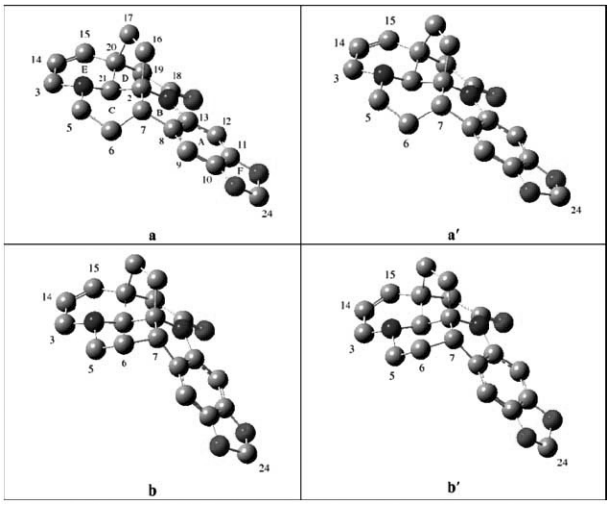

Fig. (36). B3PW91/TZ2P structures of the four conformations of (2*R*,7*S*,20*S*,21*S*)-**16**. Reprinted with permission from ref. 64. Copyright 2007 American Chemical Society.

TDDFT calculations of the ECD spectra of the four conformers of (2*R*,7*S*,20*S*,21*S*)-**16** were performed at the B3LYP/aug-cc-pVDZ//B3LYP/6-31G*, B3LYP/aug-cc-pVDZ//B3LYP/TZ2P, and B3LYP/aug-cc-pVDZ//B3PW91/TZ2P levels, all affording similar results. The small differences between length and velocity rotational strengths confirm that the aug-cc-pVDZ basis set is a good approximation to the basis set limit. The calculated ECD spectra of conformations **16a** and **16a'** are similar, as are the spectra of conformations **16b** and **16b'**, which differ significantly from those of the former. The conformationally averaged ECD spectra of (2*R*,7*S*,20*S*,21*S*)-**16**, based on the B3PW91/TZ2P geometries, are compared to the experimental spectrum in Fig. (**37**). The three calculated principal features at wavelengths around 300, 270, and 240 nm with positive, negative, and positive signs, respectively, in qualitative agreement with the experimental spectrum exhibiting positive, negative, and positive features at 317, 268 and 232 nm, allowed the AC assignment of this compound. In this study [64], theoretical calculation of optical rotations and VCD spectrum of **16** were also performed, providing convincing evidence for the AC assignment of this compound.

3.8. Dihydroxanthenones

In contrast to the above discussed examples where the experimental CD spectra were recorded in solution, a solid-state CD/TDDFT approach was successfully employed to determine the AC of globosuxanthone A (**17**) (Fig. **38**), a cytotoxic dihydroxan-

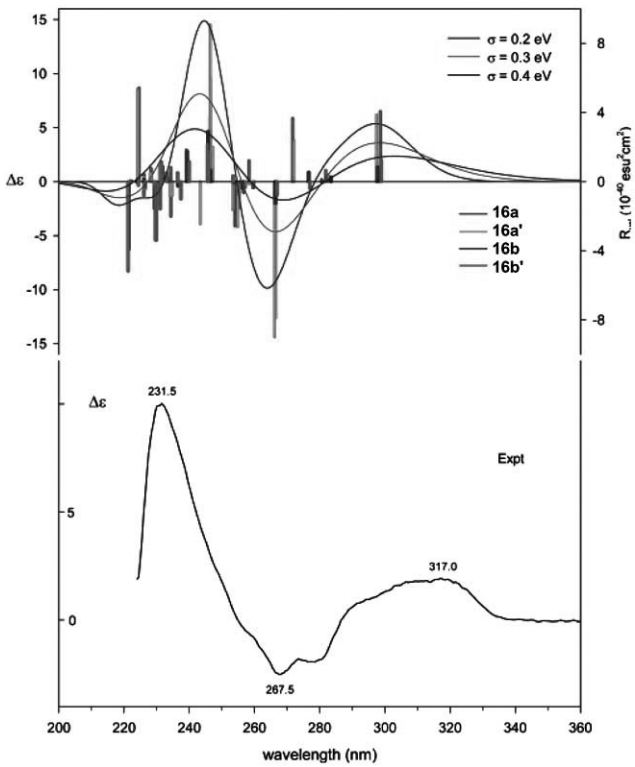

Fig. (37). Comparison of B3LYP/aug-cc-pVDZ//B3PW91/TZ2P population-weighted velocity rotational strengths of the conformations of (2*R*,7*S*,20*S*,21*S*)-**16** and the conformationally averaged ECD spectra, simulated using Gaussian band shapes (σ = 0.2, 0.3, and 0.4 eV), to the experimental ECD spectrum. Reprinted with permission from ref. [64]. Copyright 2007 American Chemical Society.

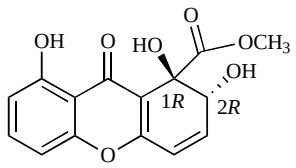

Fig. (38). Structure of globosuxanthone A (**17**).

thenone isolated from the endophytic fungi *Chaetomium globosum* and *Microdiplodia* sp. whose relative configuration was established by X-ray crystallography [65].

A solid-state ECD spectrum of **17** was acquired by using 0.13 mg sample mixed with 180.3 mg KCl. Despite some differences, the overall patterns of the solution and solid-state ECD spectra are similar for this particular compound presumably due to restrained conformation (Fig. **39**). Using the X-ray coordinates and a chosen configuration (1*R*,2*R*), TDDFT calculations of its ECD at the B3LYP/TZVP and PBE0/TZVP levels were performed and the simulated spectra are shown in Fig. (**40**). It appears that the B3LYP/TZVP level better reproduces the main experimental features above 250 nm, in terms of wavelenth, sign, and amplitude of bands, including the weakest ones (shoulders at 303 and 326 nm).

The advantage of this approach is the elimination of the conformational analysis step. A more recent example illustrated the assignment of the chiral axis of the natural product dioncophylline A using the TDDFD/B3LYP method and the more advanced DFT/MRCI approach [97]. However, X-ray crystallography data is required to provide a starting conformation that would closely

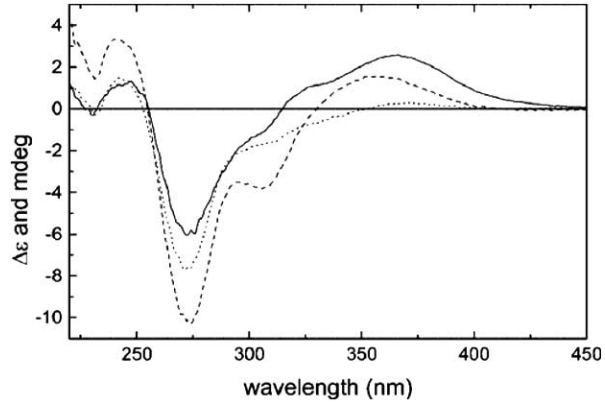

Fig. (39). ECD spectra of **17** measured in MeOH (dotted line), in MeCN/CH_2Cl_2/MeOH 1:1:1 (dashed line), and as KCl disc (solid line, in mdeg units). Reproduced with permission from ref. [65]. Copyright Wiley-VCH Verlag GmbH & Co. KGaA.

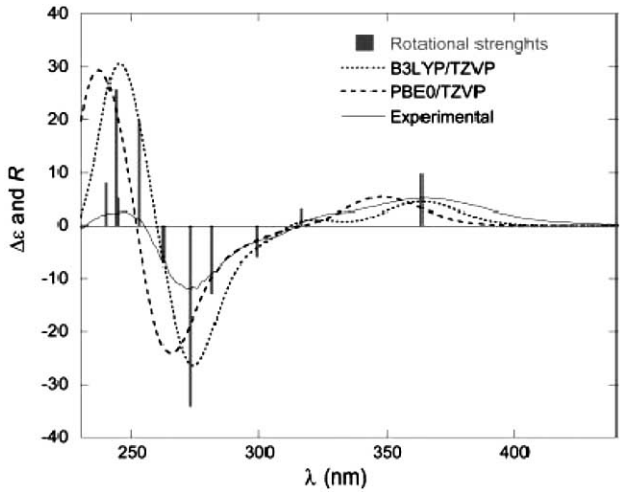

Fig. (40). ECD spectra of **17**: experimental as KCl disc (solid line, multiplied by two), and computed with TDDFT with use of B3LYP/TZVP (dotted line) and PBE0/TZVP (dashed line). Vertical bars represent B3LYP-computed rotational strengths in 10^{-40} cgs units. Reproduced with permission from ref. [65]. Copyright Wiley-VCH Verlag GmbH & Co. KGaA.

mimic the 'solid' conformation in the ECD measurement. In the case of a complex molecule with significant conformational flexibility where X-ray crystallography can only determine the relative configuration, this approach would be efficient and effective for AC assignment.

4. CONCLUSIONS

It is a chemists' dream that a straightforward, non-destructive, easy to implement *in silico* method can be used to determine the AC of natural products. It appears that the TDDFD calculation of ECD spectra has emerged as a very promising tool in this regard. The fundamental issue of this approach is to utilize the conformers that best reflect their preferred conformations in solution. Generally, conformationally rigid molecules that possess restrained conformations will produce more reliable results, while conformationally flexible molecules require considerable efforts for conformational analysis and calculations. In most cases, conclusions for unambiguous configurational assignment can be drawn, even though the calculated ECD spectra do not perfectly match the experimental ones. However, cautions should be taken as minor conformational

changes in some cases may cause significant changes of the calculated ECD spectra. Although ECD data may not provide complete stereochemical information of a structurally complex natural product with multiple stereogenic centers, the sensitivity of experimental ECD and simplicity of theoretical calculation highlights its advantages in determining the AC of natural products. ECD calculations may be further complemented by other chiroptical methods such as calculation of optical rotation values and VCD spectra. With the continued advancement of the computational technologies, it is expected that ECD calculations will become a routine tool for natural product chemists for AC assignment.

ACKNOWLEDGMENTS

This work was supported in part by the USDA Agricultural Research Service Specific Cooperative Agreement No. 58-6408-2-0009 and NIH AI 027094.

REFERENCES

[1] Mechlinski, W.; Schaffner, C.P.; Ganis, P.; Avitabile, G. Structure and absolute configuration of the polyene macrolide antibiotic amphotericin B. *Tetrahedron Lett.,* **1970**, *44*, 3873-3876.

[2] Flack, H. D. On enantiomorph-polarity estimation. *Acta Crystallogr. Sect. A, 39*, **1983**, 876-881.

[3] Flack, H. D.; Bernardinelli, G. Reporting and evaluating absolute-structure and absolute-configuration determinations. *J. Appl. Crystallogr.,* **2000**, *33*, 1143-1148.

[4] Hooft, R. W. W.; Straver, L. H.; Spek, A. L. Determination of absolute structure using Bayesian statistics on Bijvoet differences. *J. Appl. Crystallogr.,* **2008**, *41*, 96-103.

[5] Kamel, H. N.; Ding, Y. Q.; Li, X. C.; Ferreira, D.; Fronczek, F. R.; Slattery, M. Beyond polymaxenolide: cembrane-Africanane terpenoids from the hybrid soft coral *Sinularia maxima* × *S. polydactyla* *J. Nat. Prod*., **2009**, *72*, 900-905.

[6] Fu, X.; Li, X.-C.; Smillie , T. A.; Carvalho, P.; Mabusela, W.; Syce, J.; Johnson, Q.; Folk, W.; Avery, M. A.; Khan, I. A. Cycloartane glycosides from *Sutherlandia frutescens*. *J. Nat. Prod*., **2008**, *71*, 1749-1753.

[7] Nicolaou, K. C.; Daines, R. A.; Ogawa, Y.; Chakraborty, T. K. *J.* Total synthesis of amphotericin B. 3. The final stages. *J. Am. Chem. Soc.,* **1988**, *110*, 4696-4705.

[8] Nicolaou, K. C.; Yang, Z.; Liu, J. J.; Ueno, H.; Nantermet, P. G.; Guy, R. K.; Claiborne, C. F.; Renaud, J.; Couladouros, E. A.; Paulvannan, K.; Sorensen, E. J. Total synthesis of taxol. *Nature,* **1994**, *367*, 630-634.

[9] Seco, J. M.; Quiñoá, E.; Riguera, R. The assignment of absolute configuration by NMR. *Chem. Rev.,* **2004**, *104*, 17-117.

[10] Dale, J. A.; Mosher, H. S. Nuclear magnetic resonance enantiomer regents. Configurational correlations via nuclear magnetic resonance chemical shifts of diastereomeric mandelate, *O*-methylmandelate, and α-methoxy-α-trifluoromethylphenylacetate (MTPA) esters. *J. Am. Chem. Soc.,* **1973**, *95*, 512-519.

[11] Adams, C. M.; Indranath Ghosh, I.; Kishi, Y. Validation of lanthanide chiral shift reagents for determination of absolute configuration: total synthesis of glisoprenin A. *Org. Lett.,* **2004**, *6*, 4723-4726.

[12] Buist, P. H.; Dale Marecak, D.; Holland, H. L.; Brown, F. M. (*S*)-α-Methoxyphenyl acetic acid: a new NMR chiral shift reagent for the stereochemical analysis of sulfoxides. *Tetrahedron Asymmetry* **1995**, *6*, 7-10.

[13] B'Hymer, C.; Montes-Bayon, M.; Caruso, J. A. Marfey's reagent: Past, present, and future uses of 1-fluoro-2,4-dinitrophenyl-5-L-alanine amide. *J. Separ. Sci.* **2003**, *26*, 7-19.

[14] Hara, S.; Okabe, H.; Mihashi, K. Gas-liquid chromatographic separation of aldose enantiomers as trimethylsilyl ethers of methyl 2-(polyhydroxyalkyl)thiazolidine-4(R)-carboxylates. *Chem. Pharm. Bull.,* **1987**, *35*, 501-506.

[15] Tanaka, T.; Nakashima, T.; Ueda, T.; Tomii, K.; Kouno, I. Facile discrimination of aldose enantiomers by reversed-phase HPLC. *Chem. Pharm. Bull.,* **2007**, *55*, 899-901.

[16] Klyne, W. The configuration of the anomeric carbon atoms in some cardiac glycosides. *Biochem. J.,* **1950**, *47*, xli-xlii.

[17] Barton, D. H. R. Application of the method of molecular rotation differences to steroids. I. Naturally occurring sterols and their simple derivatives. *J. Chem. Soc.,* **1945**, 813-819.

[18] Moffitt, W.; Woodward, R. B.; Moscowitz, A.; Klyne, W.; Djerassi, C. Structure and the optical rotatory dispersion of saturated ketones. *J. Am. Chem. Soc.,* **1961**, *83*, 4013-4018.

[19] Moscowitz, A.; Mislow, K.; Glass, M. A. W.; Djerassi, C. Optical rotatory dispersion studies. LXVI. Optical rotatory dispersion associated with dissymmetric nonconjugated chromophores. An extension of the octant rule. *J. Am. Chem. Soc.,* **1962**, *84*, 1945-1955.

[20] DeAngelis, G. G.; Wildman, W. C. Circular dichroism studies. I. A quadrant rule for the optically active aromatic chromophore in rigid polycyclic systems. *Tetrahedron,* **1969**, *25*, 5099-5112.

[21] Harada, N.; Nakanishi, K. Circular Dichroic Spectroscopy-Exciton Coupling in Organic Stereochemistry; University Science Books: Mill Valley, CA, **1983**.

[22] Harada, N.; Kohori, J.; Uda, H.; Toriumi, K. Synthesis, absolute stereochemistry, and circular dichroism of chiral 1,8a-dihydroazulene derivatives. *J. Org. Chem.,* **1989**, *54*, 1820-1826.

[23] Harada, N.; Uda, H.; Kobayashi, M.; Shimizu, N.; Kitagawa, I. Absolute stereochemistry of the halenaquinol family, marine natural products with a novel pentacyclic skeleton, as determined by the theoretical calculation of circular dichroism spectra. *J. Am. Chem. Soc.,* **1989**, *111*, 5668-5674.

[24] Ferris, J. P.; Boyce, C. B.; Briner, R. C.; Weiss, U.; Qureshi, I. H.; Sharpless, N. E. Lythraceae alkaloids. X. Assignment of absolute stereochemistries on the basis of chiraloptical effects. *J. Am. Chem. Soc.,* **1971**, *93*, 2963-2968.

[25] Slade, D.; Ferreira, D.; Marais, J. P. J. Circular dichroism, a powerful tool for the assessment of absolute configuration of flavonoids. *Phytochemistry,* **2005**, *66*, 2177-2215.

[26] Rodger, A.; Nordén, B. Circular Dichroism and Linear Dichroism, Oxford University Press: Oxford, UK, **1997**.

[27] Fasman, G. D. Circular Dichroism and the Conformational Analysis of Biomolecules, Plenum Press: New York, **1996**.

[28] Berova, N.; Nakanishi, K. *Circular Dichroism Principles and Applications*; Berova, N.; Nakanishi, K.; Woody, R. W. Eds.; John Wiley & Sons: New York, **2000**; Chapter 12, pp. 337-382.

[29] Berova, N.; Bari, L. D.; Pescitelli, G. Application of electronic circular dichroism in configurational and conformational analysis of organic compounds. *Chem. Soc. Rev.,* **2007**, *36*, 914-931.

[30] Gaffield, W. Circular dichroism, optical rotatory dispersion, and absolute configuration of flavanones, 3-hydroxyflavanones, and their glycosides. Determination of aglycone chirality in flavanone glycosides. *Tetrahedron,* **1970**, *26*, 4093-4108.

[31] Diedrich, C.; Grimme, S. Systematic investigation of modern quantum chemical methods to predict electronic circular dichroism spectra. *J. Phys. Chem. A,* **2003**, *107*, 2524-2539.

[32] Stephens, P. J.; McCann, D. M.; Butkus, E.; Stoncius, S.; Cheeseman, J. R.; Frisch, M. J. Determination of absolute configuration using concerted ab initio DFT calculations of electronic circular dichroism and optical rotation: bicyclo[3.3.1]nonane diones. *J. Org. Chem.,* **2004**, *69*, 1948-1958.

[33] Stephens, P. J.; McCann, D. M.; Devlin, F. J.; Cheeseman, J. R.; Frisch, M. J. Determination of the absolute configuration of [3(2)](1,4)barrelenophanedicarbonitrile using concerted time-dependent density functional theory calculations of optical rotation and electronic circular dichroism. *J. Am. Chem. Soc.,* **2004**, *126*, 7514-7521.

[34] Schühly, W.; Crochett, S. L.; Fabian, W. M. F. Hyperolactone C: Determination of its absolute configuration by comparison of experimental and calculated CD spectra. *Chirality,* **2005**, *17*, 250-256.

[35] McCann, D. M.; Stephens, P. J. Determination of absolute configuration using density functional theory calculations of optical rotation and electronic circular dichroism: chiral alkenes. *J. Org. Chem.,* **2006**, *71*, 6074-6098.

[36] Crawford, T. D.; Tam, M. C.; Abrams, M. L. The current state of ab initio calculations of optical rotation and electronic circular dichroism spectra. *J. Phys. Chem. A,* **2007**, *111*, 12057-12068.

[37] Stephens, P. J.; Devlin, F. J.; Gasparrini, F.; Ciogli, A.; Spinelli, D.; Cosimelli, B. Determination of the absolute configuration of a chiral oxadiazol-3-one calcium channel blocker, resolved using chiral chromatography, via concerted density functional theory calculations of its vibrational circular dichroism, electronic circular dichroism, and optical rotation. *J. Org. Chem.,* **2007**, *72*, 4707-4715.

[38] Ding, Y.; Li, X.-C.; Ferreira, D. Theoretical calculation of electronic circular dichroism of the rotationally restricted 3,8"-biflavonoid morelloflavone. *J. Org. Chem.,* **2007**, *72*, 9010-9017.

[39] Bringmann, G.; Bruhn, T.; Maksimenka, K.; Hemberger, Y. The assignment of absolute stereostructures through quantum chem. circular dichroism calculations. *Eur. J. Org. Chem.,* **2009**, 2717-2727.

[40] Stephens, P. J.; Devlin, F. J.; Cheeseman, J. R.; Frisch, M. J. Calculation of optical rotation using density functional theory. *J. Phys. Chem. A,* **2001**, *105*, 5356-5371.

[41] Polavarapu, P. L. Optical rotation: recent advances in determining the absolute configuration. *Chirality,* **2002**, *14*, 768-781.

[42] Stephens, P. J.; Devlin, F. J.; Cheeseman, J. R.; Frisch, M. J. Ab initio prediction of optical rotation: comparison of density functional theory and Hartree-Fock methods for three 2,7,8-trioxabicyclo[3.2.1]octanes. *Chirality,* **2002**, *14*, 288-296.

[43] Stephens, P. J.; Devlin, F. J.; Cheeseman, J. R.; Frisch, M. J.; Bortolini, O.; Besse, P. Determination of absolute configuration using ab initio calculation of optical rotation. *Chirality,* **2003**, *15*, S57-S64.

[44] McCann, D. M.; Stephens, P. J.; Cheeseman, J. R. Determination of absolute configuration using density functional theory calculation of optical rotation: chiral alkanes. *J. Org. Chem.,* **2004**, *69*, 8709-8717.

[45] Giorgio, E.; Roje, M.; Tanaka, K.; Hamersak, Z.; Sunjik, V.; Nakanishi, K.; Rosini, C.; Berova, N. Determination of the absolute configuration of flexible molecules by ab initio ORD calculations: a case study with cytoxazones and isocytoxazones. *J. Org. Chem.,* **2005**, *70*, 6557-6563.

[46] Stephens, P. J.; Pan, J. J.; Devlin, F. J.; Cheeseman, J. R. Determination of the absolute configurations of natural products using TDDFT optical rotation calculations: the iridoid oruwacin. *J. Nat. Prod.,* **2008**, *71*, 285-288.

[47] Aamouche, A.; Devlin, F. J.; Stephens, P. J. Determination of absolute configuration using circular dichroism: Troger's base revisited using vibrational circular dichroism. *Chem. Commun.,* **1999**, 361-362.

[48] Aamouche, A.; Devlin, F. J.; Stephens, P. J. Structure, vibrational absorption and circular dichroism spectra, and absolute configuration of Troger's base. *J. Am. Chem. Soc.,* **2000**, *122*, 2346-2354.

[49] Devlin, F. J.; Stephens, P. J.; Oesterle, C.; Wiberg, K. B.; Cheeseman, J. R.; Frisch, M. J. Configurational and conformational analysis of chiral molecules using IR and VCD spectroscopies: spiropentylcarboxylic acid methyl ester and spiropentyl acetate. *J. Org. Chem.,* **2002**, *67*, 8090-8096.

[50] Freedman, T. B.; Cao, X.; Dukor, R. K.; Nafie, L. A. Absolute configuration determination of chiral molecules in the solution state using vibrational circular dichroism. *Chirality* **2003**, *15*, 743-758.

[51] Stephens, P. J.; McCann, D. M.; Devlin, F. J.; Flood, T. C.; Butkus, E.; Stoncius, S.; Cheeseman, J. R. Determination of molecular structure using vibrational circular dichroism spectroscopy: the keto-lactone product of Baeyer-Villiger oxidation of (+)-(1R,5S)-bicyclo[3.3.1]nonane-2,7-dione. *J. Org. Chem.,* **2005**, *70*, 3903-3913.

[52] Carosati, E.; Cruciani, G.; Chiarini, A.; Budriesi, R.; Ioan, P.; Spisani, R.; Spinelli, D.; Cosimelli, B.; Fusi, F.; Frosini, M.; Matucci, R.; Gasparrini, F.; Ciogli, A.; Stephens, P. J.; Devlin, F. J. Calcium channel antagonists discovered by a multidisciplinary approach. *J. Med. Chem.,* **2006**, *49*, 5206-5216.

[53] Monde, K.; Taniguchi, T.; Miura, M.; Vairappan, C. S.; Suzuki, M. Absolute configurations of endoperoxides determined by vibrational circular dichroism (VCD). *Tetrahedron Lett.,* **2006**, *47*, 4389-4392.

[54] Cerda-García-Rojas, C. M.; Catalán, C. A. N.; Muro, A. C.; Joseph-Nathan, P. Vibrational circular dichroism of Africanane and lippifoliane sesquiterpenes from *Lippia integrifolia*. *J. Nat. Prod.,* **2008**, *71*, 967-971.

[55] Crawford, T. D.; Tam, M. C.; Abrams, M. L. The problematic case of (*S*)-methylthiirane: electronic circular dichroism spectra and optical rotatory dispersion. *Mol. Phys.,* **2007**, *105*, 2607-2617.

[56] Skomorowski, W.; Pecul, M.; Salek, P.; Helgaker, T. Electronic circular dichroism of disulphide bridge: ab initio quantum-chemical calculations. *J. Chem. Phys.,* **2007**, *127*, 085102/1-085102/8.

[57] Pecul, M.; Ruud, K. The ab initio calculation of optical rotation and electronic circular dichroism. *Adv. Quant. Chem.* **2005**, *50*, 185-212.

[58] Kwit, M.; Sharma, N.D.; Boyd, D. R.; Gawronski, J. Absolute configuration of conformationally flexible cis-dihydrodiol metabolites by the method of confrontation of experimental and calculated electronic CD spectra and optical rotations. *Chem-Eur. J.,* **2007**, *13*, 5812-5821.

[59] Mori, T.; Inoue, Y.; Grimme, S. Quantum chemical study on the circular dichroism spectra and specific rotation of donor-acceptor cyclophanes. *J. Phys. Chem. A,* **2007**, *111*, 7995-8006.

[60] Giorgio, E.; Tanaka, K.; Ding, W.; Krishnamurthy, G.; Pitts, K.; Ellestad, G. A.; Rosini, C.; Berova, N. Theoretical simulation of the electronic circular dichroism spectrum of calicheamicin. *Bioorg. Med. Chem.,* **2005**, *13*, 5072-5079.

[61] Gawronski, J. K.; Kwit, M.; Boyd, D. R.; Sharma, N. D.; Malone, J. F.; Drake, A. F. Absolute configuration, conformation, and circular dichroism of monocyclic arene dihydrodiol metabolites: it is all due to the heteroatom substituents. *J. Am. Chem. Soc.,* **2005**, *127*, 4308-4319.

[62] Stephens, P. J.; McCann, D. M.; Devlin, F. J.; Smith, A. B., III. Determination of the absolute configurations of natural products via density functional theory calculations of optical rotation, electronic circular dichroism, and vibrational circular dichroism: the cytotoxic sesquiterpene natural products quadrone, suberosenone, suberosanone, and suberosenol A acetate. *J. Nat. Prod.,* **2006**, *69*, 1055-1064.

[63] Stephens, P. J.; Pan, J. J.; Devlin, F. J.; Krohn, K.; Kurtan, T. Determination of the absolute configurations of natural products via density functional theory calculations of vibrational circular dichroism, electronic circular dichroism, and optical rotation: the iridoids plumericin and isoplumericin. *J. Org. Chem.,* **2007**, *72*, 3521-3536.

[64] Stephens, P.J.; Pan, J. J.; Devlin, F. J.; Urbanova, M.; Hajicek, J. Determination of the absolute configurations of natural products via density functional theory calculations of vibrational circular dichroism, electronic circular dichroism and optical rotation: the schizozygane alkaloid schizozygine. *J. Org. Chem.,* **2007**, *72*, 2508-2524.

[65] Hussain, H.; Krohn, K.; Floerke, U.; Schulz, B.; Draeger, S.; Pescitelli, G.; Antus, S.; Kurtán, T. Absolute configurations of globosuxanthone A and secondary metabolites from *Microdiplodia* sp. - a novel solid-state CD/TDDFT approach. *Eur. J. Org. Chem.,* **2007**, 292-295.

[66] Stephens, P. J.; Pan, J.-J.; Devlin, F. J.; Urbanova, M.; Julinek, O.; Hajicek, J. Determination of the absolute configurations of natural products via density functional theory calculations of vibrational circular dichroism, electronic circular dichroism, and optical rotation: the iso-schizozygane alkaloids isoschizogaline and isoschizogamine. *Chirality,* **2008**, *20*, 454-470.

[67] Bringmann, G.; Gulder, T. A. M.; Reichert, M.; Gulder, T. The online assignment of the absolute configuration of natural products: HPLC-CD in combination with quantum chemical CD calculations. *Chirality,* **2008**, *20*, 628-642.

[68] Grkovic, T.; Ding, Y.; Li, X. C.; Webb, V. L.; Ferreira, D.; Copp, B. R. Enantiomeric discorhabdin alkaloids and establishment of their absolute configurations using theoretical calculations of electronic circular dichroism spectra. *J. Org. Chem.,* **2008**, *73*, 9133-9136.

[69] Ross, S. A.; Rodriguez-Guzman, R.; Radwan, M. M.; Jacob, M. R.; Ding, Y. Q.; Li, X. C., Ferreira, D.; Manly, S. P.; Sorocenol, G. H. Sorocenols G and H, anti-MRSA oxygen heterocyclic Diels-Alder-type adducts from Sorocea muriculata roots. *J. Nat. Prod.,* **2008**, *71*, 1764-1767.

[70] Ding, Y.; Li, X. C.; Ferreira, D. Theoretical calculation of electronic circular dichroism of a hexahydroxydiphenoyl-containing flavanone glycoside. *J. Nat. Prod.,* **2009**, *72*, 327-335.

[71] Shukla, Y. J.; Pawar, R. S.; Ding, Y.; Li, X. C.; Ferreira, D.; Khan, I. A. Pregnane glycosides from *Hoodia gordonii*. *Phytochemistry,* **2009**, *70*, 675-683.

[72] Yang, X.-W.; Ding, Y.; Li, X.-C.; Ferreira, D.; Shen, Y.-H.; Li, S. M.; Wang, N.; Zhang, W.-D. Cycloabiesesquine A, a unique sesquiterpenoid from *Abies delavayi*. *Chem. Commun.,* **2009**, *25*, 3771-3773.

[73] Li, J.; Ding, Y.; Li, X.-C.; Ferreira, D.; Khan, S. I.; Smillie, T. J.; Khan, I. A. Scuteflorins A and B, dihydropyranocoumarins from *Scutellaria lateriflora*. *J. Nat. Prod.,* **2009**, *72*, 983-987.

[74] Taniguchi, T.; Martin, C. L.; Monde, K.; Nakanishi, K.; Berova, N.; Overman, L. E. Absolute configuration of actinophyllic acid as determined through chiroptical data. *J. Nat. Prod.,* **2009**, *72*, 430-432.

[75] Gan, L.-S.; Zheng, Y.-L.; Mo, J.-X.; Liu, X.; Li, X.-H.; Zhou, C.-X. Sesquiterpene lactones from the root tubers of *Lindera aggregata*. *J. Nat. Prod.,* **2009**, *72*, 1497-1501.

[76] Petrovic, A. G.; He, J.; Polavarapu, P. L.; Xiao, L. S.; Armstrong, D. *W.* Absolute configuration and predominant conformations of 1,1-dimethyl-2-phenylethyl phenyl sulfoxide. *Org. Biomol. Chem.,* **2005**, *3*, 1977-1981.

[77] Claps, M.; Parrinello, N.; Saa, C.; Varela, *J. A.; Caccamese,* **S.;** Rosini, C. Assignment of the absolute configuration of (+)-5,5',6,6'-tetrahydro-7,7'-spiro[7H-cyclopenta[b]pyridine], a new inherently chiral spiropyridine, by a nonempirical analysis of its circular dichroism spectrum. *Tetrahedron Asymmetry* **2006**, *17*, 1387-1393.

[78] Giorgio, E.; Tanaka, K.; Verotta, L.; Nakanishi, K.; Berova, N.; Rosini, C. Determination of the absolute configurations of flexible molecules: synthesis and theoretical simulation of electronic circular dichroism/optical rotation of some pyrrolo[2,3-b]indoline alkaloids - a case study. *Chirality,* **2007**, *19*, 434-445.

[79] Tanaka, T.; Oelgemoller, M.; Fukul, K.; Aoki, F.; Mori, T.; Ohno, T.; Inoue, Y. Unusual CD couplet pattern observed for the pi*←n transition of enantiopure (Z)-8-methoxy-4-cyclooctenone: an experimental and theoretical study by electronic and vibrational circular dichroism spectroscopy and density functional theory calculation. *Chirality,* **2007**, *19*, 415-427.

[80] Ding, S.; Jia, L.; Durandin, A.; Crean, C.; Kolbanovskiy, A.; Shafirovich, V.; Broyde, S.; Geacintov, N. E. Absolute configurations of spiroiminodihydantoin and allantoin stereoisomers: comparison of computed and measured electronic circular dichroism spectra. *Chem. Res. Toxicol.,* **2009**, *22*, 1189-1193.

[81] Bicker, W.; Kacprzak, K.; Kwit, M.; Laemmerhofer, M.; Gawronski, J.; Lindner, W. Assignment of absolute configurations of permethrin and its synthon 3-(2,2-dichlorovinyl)-2,2-dimethylcyclopropanecarboxylic acid by electronic circular dichroism, optical rotation, and X-ray crystallography. *Tetrahedron Asymmetry,* **2009**, *20*, 1027-1035.

[82] Sybyl 8.0; Tripos Inc., www.tripos.com.

[83] Spartan 02; Wavefunction, Inc.; www.wafefun.com.

[84] Gaussian03, Gaussian, Inc., www.gaussian.com.

[85] Pecul, M.; Ruud, K.; Helgaker, T. Density functional theory calculation of electronic circular dichroism using London orbitals. *Chem. Phys. Lett.,* **2004**, *388*, 110-119.

[86] Klamt, A.; Schürmann, G. COSMO: a new approach to dielectric screening in solvents with explicit expressions for the screening energy and its gradient. *J. Chem. Soc., Perkin Trans. 2,* **1993**, *2*, 799-805.

[87] Klamt, A. Conductor-like screening model for real solvents: a new approach to the quantitative calculation of solvation phenomena. *J. Phys. Chem.,* **1995**, *99*, 2224-2235.

[88] Eckert, F.; Klamt, A. Fast solvent screening via quantum chemistry: COSMO-RS approach. *AIChE J.,* **2002**, *48*, 369-385.

[89] Al-Basheer, W.; Pagni, R. M.; Compton, R. N. Spectroscopic and theoretical investigation of (*R*)-3-methylcyclopentanone. The effect of solvent and temperature on the distribution of conformers. *J. Phys. Chem. A,* **2007**, *111*, 2293-2298.

[90] Mori, T.; Inoue, Y.; Grimme, S. Time dependent density functional theory calculations for electronic circular dichroism spectra and optical rotations of conformationally flexible chiral donor-acceptor dyad. *J. Org. Chem.,* **2006**, *71*, 9797-9806.

[91] Caccamese, S.; Caruso, C.; Parrinello, N.; Savarino, A. High-performance liquid chromatographic separation and chiroptical properties of the enantiomers of naringenin and other flavanones. *J. Chromatogr. A,* **2005**, *1076*, 155-162.

[92] Li, X.-C.; Joshi, A. S.; Tan, B.; ElSohly, H. N.; Walker, L. A.; Zjawiony, J. K.; Ferreira, D. Absolute configuration, conformation, and chiral properties of flavanone-(3-8´´)-flavone biflavonoids from *Rheedia acuminata*. *Tetrahedron*, **2002**, *58*, 8709-8717.

[93] Duddeck, H.; Snatzke, G.; Yemul, S. S. ^{13}C NMR and CD of some 3,8"-biflavanoids from *Garcinia* species and of related flavanones. *Phytochemistry*, **1978**, *17*, 1369-1373.

[94] Li, X.-C.; Jacob, M. R.; Pasco, D. S.; ElSohly, H. N.; Nimrod, A. C.; Walker, L. A.; Clark, A. M. Phenolic compounds from *Miconia myriantha* inhibiting *Candida* secreted aspartic proteases. *J. Nat. Prod.*, **2001**, *64*, 1282-1285.

[95] Okuda, T.; Yoshida, T.; Hatano, T.; Koga, T.; Toh, N.; Kuriyama, K. Circular dichroism of hydrolyzable tannins. I. Ellagitannins and gallotannins. *Tetrahedron Lett.*, **1982**, *38*, 3937-3940.

[96] Na, M.; Ding, Y.; Wang, B.; Tekwani, B.L.; Schinazi, R. F.; Franzblau, S.; Kelly, M.; Stone, R.; Li, X.-C.; Ferreira, D.; Hamann, M. T. Anti-infective discorhabdins from a deep-water Alaskan sponge of the genus *Latrunculia*. *J. Nat. Prod.*, **2010**, *73*, 383-387.

[97] Bringmann G.; Maksimenka K.; Bruhn T.; Reichert M.; Harada T.; Koroda R. Quantum chemical CD calculations of dioncophylline A in the solid state. *Tetrahedron*, **2009**, *65*, 5720-5728.

Received: 30 August, 2009 Revised: 13 November, 2009 Accepted: 14 November, 2009

Copyright of Current Organic Chemistry is the property of Bentham Science Publishers Ltd. and its content may not be copied or emailed to multiple sites or posted to a listserv without the copyright holder's express written permission. However, users may print, download, or email articles for individual use.